Annu. Rev. Nucl. Part. Sci. 2020.70:355-394. Downloaded from www.annualreviews.org
Access provided by WIB6263 - Deutsches Elektronen Synchroton (DESY) on 04/08/21. See copyright for approved use.

ANNUAL REVIEWS

Annual Review of Nuclear and Particle Science

Primordial Black Holes as Dark Matter: Recent Developments

Bernard Carr[1] and Florian Kühnel[2]

[1]School of Physics and Astronomy, Queen Mary University of London, London E1 4NS, United Kingdom; email: b.j.carr@qmul.ac.uk

[2]Arnold Sommerfeld Center for Theoretical Physics, Ludwig-Maximilians-Universität, 80333 München, Germany; email: kuhnel@kth.se

ANNUAL REVIEWS CONNECT

www.annualreviews.org

- Download figures
- Navigate cited references
- Keyword search
- Explore related articles
- Share via email or social media

Annu. Rev. Nucl. Part. Sci. 2020. 70:355–94

First published as a Review in Advance on August 3, 2020

The *Annual Review of Nuclear and Particle Science* is online at nucl.annualreviews.org

https://doi.org/10.1146/annurev-nucl-050520-125911

Copyright © 2020 by Annual Reviews. This work is licensed under a Creative Commons Attribution 4.0 International License, which permits unrestricted use, distribution, and reproduction in any medium, provided the original author and source are credited. See credit lines of images or other third party material in this article for license information

OPEN ACCESS CC BY

Keywords

black holes, dark matter, gravitational waves, cosmic structure

Abstract

Although the dark matter is usually assumed to be made up of some form of elementary particle, primordial black holes (PBHs) could also provide some of it. However, various constraints restrict the possible mass windows to 10^{16}–10^{17} g, 10^{20}–10^{24} g, and 10–$10^3 M_\odot$. The last possibility is contentious but of special interest in view of the recent detection of black hole mergers by LIGO/Virgo. PBHs might have important consequences and resolve various cosmological conundra even if they account for only a small fraction of the dark matter density. In particular, those larger than $10^3 M_\odot$ could generate cosmological structures through the seed or Poisson effect, thereby alleviating some problems associated with the standard cold dark matter scenario, and sufficiently large PBHs might provide seeds for the supermassive black holes in galactic nuclei. More exotically, the Planck-mass relics of PBH evaporations or stupendously large black holes bigger than $10^{12} M_\odot$ could provide an interesting dark component.

Annu. Rev. Nucl. Part. Sci. 2020.70:355-394. Downloaded from www.annualreviews.org
Access provided by WIB6263 - Deutsches Elektronen Synchroton (DESY) on 04/08/21. See copyright for approved use.

Contents

1. INTRODUCTION

Primordial black holes (PBHs) have been a source of interest for nearly 50 years (1) even though there is still no evidence for them. One reason for this interest is that only PBHs could be small enough for Hawking radiation to be important (2). This discovery has not yet been confirmed experimentally, and there remain major conceptual puzzles associated with the process. Nevertheless, it is generally recognized as one of the key developments in twentieth-century physics because it beautifully unifies general relativity, quantum mechanics, and thermodynamics. The fact that Hawking reached this discovery only through contemplating the properties of PBHs illustrates that it can be useful to study something even if it does not exist. But, of course, the situation is much more interesting if PBHs do exist.

PBHs smaller than about 10^{15} g would have evaporated by now with many interesting cosmological consequences (3). Studies of such consequences have placed useful constraints on models of the early Universe, and, more positively, evaporating PBHs have been invoked to explain certain features, such as the extragalactic (4) and Galactic (5) γ-ray backgrounds, antimatter in cosmic

rays (6), the annihilation line radiation from the Galactic center (7), the reionization of the pregalactic medium (8), and some short-period γ-ray bursts (9). However, there are other possible explanations for most of these features, so there is no definitive evidence for evaporating PBHs. Only the original papers for each topic are cited here; a more comprehensive list of references can be found in Reference 3.

Attention has therefore shifted to PBHs larger than 10^{15} g, which are unaffected by Hawking radiation. Such PBHs might have various astrophysical consequences, such as the seeding of supermassive black holes (SMBHs) in galactic nuclei (10), the generation of large-scale structure through Poisson fluctuations (11), and important effects on the thermal and ionization history of the Universe (12). Again, only the original papers are cited here. But perhaps the most exciting possibility—and the main focus of this review—is that PBHs could provide the dark matter that accounts for 25% of the critical density (13), an idea that goes back to the earliest days of PBH research (14). Because PBHs formed in the radiation-dominated era, they are not subject to the well-known big bang nucleosynthesis (BBN) constraint that baryons can have at most 5% of the critical density (15). They should therefore be classified as nonbaryonic and behave like any other form of cold dark matter (CDM) (16). It is sometimes assumed that they must form before BBN, implying an upper limit of $10^5 M_\odot$, but the fraction of the Universe in PBHs at that time would be tiny, so the effect on BBN might only be small.

As with other CDM candidates, there is still no compelling evidence that PBHs provide the dark matter. However, there have been claims of evidence from dynamical and lensing effects. In particular, there was a flurry of excitement in 1997, when the MACHO microlensing results (17) suggested that the dark matter might comprise compact objects of mass $0.5 M_\odot$. Alternative microlensing candidates could be excluded, and PBHs of this mass might naturally form at the quark–hadron phase transition at 10^{-5} s (18). Subsequently, however, it was shown that such objects could account for only 20% of the dark matter, and indeed, the entire mass range of 10^{-7} to $10 M_\odot$ was later excluded from providing all of it (19). In recent decades, attention has focused on other mass ranges in which PBHs could have a significant density, and numerous constraints allow only three possibilities: the asteroid mass range (10^{16}–10^{17} g), the sublunar mass range (10^{20}–10^{26} g), and the intermediate mass range (10–$10^3 M_\odot$).

We discuss the constraints on $f(M)$, the fraction of the halo in PBHs of mass M, in Section 3; this discussion is a much-reduced version of the recent review by Carr et al. (20). The results are summarized in **Figure 1**; all the limits assume that the PBHs have a monochromatic mass function and cluster in the Galactic halo in the same way as other forms of CDM. Although, for the sake of completeness, we include evaporating PBHs, we do not focus on them in this review except insomuch as they may leave stable Planck-mass relics because these could also be dark matter candidates. However, it is worth stressing that if Hawking evaporation were avoided for some reason, PBHs could provide the dark matter all the way down to the Planck mass with few (if any) nongravitational constraints.

At first sight, **Figure 1** implies that PBHs are excluded from having an appreciable density in almost every mass range. However, our intention is not to put nails in the coffin of the PBH scenario because every constraint is a potential signature. In particular, there are still some mass windows in which PBHs could provide the dark matter. PBHs could be generated by inflation in all of these windows, but theorists are split as to which one they favor. For example, Inomata et al. (21) argue that double inflation can produce a peak at around 10^{20} g, while Clesse & García-Bellido (22) argue that hybrid inflation can produce a peak at around $10 M_\odot$. A peak at the latter mass could also be produced by a reduction in the pressure at the quark–hadron phase transition (23) even if the primordial fluctuations have no feature on that scale. There is a parallel here with

Annu. Rev. Nucl. Part. Sci. 2020.70:355-394. Downloaded from www.annualreviews.org
Access provided by WIB6263 - Deutsches Elektronen Synchroton (DESY) on 04/08/21. See copyright for approved use.

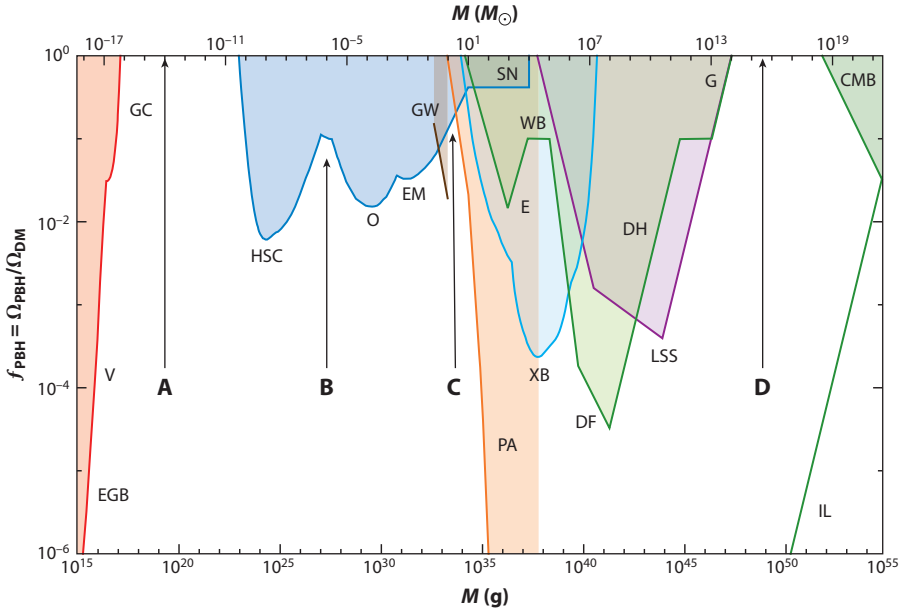

Figure 1

Constraints on $f(M)$ for a monochromatic mass function from evaporations (*red*), lensing (*dark blue*), gravitational waves (GW) (*brown*), dynamical effects (*green*), accretion (*light blue*), cosmic microwave background distortions (*orange*), and large-scale structure (*purple*). Evaporation limits come from the extragalactic γ-ray background (EGB), the Voyager positron flux (V), and annihilation line radiation from the Galactic center (GC). Lensing limits come from microlensing of supernovae (SN) and of stars in M31 by the Subaru Hyper Suprime-Cam (HSC), the Magellanic Clouds by EROS and MACHO (EM), and the Galactic bulge by OGLE (O). Dynamical limits come from wide binaries (WB), star clusters in Eridanus II (E), halo dynamical friction (DF), galaxy tidal distortions (G), heating of stars in the Galactic disc (DH), and the cosmic microwave background dipole (CMB). Large-scale structure constraints derive from the requirement that various cosmological structures do not form earlier than observed (LSS). Accretion limits come from X-ray binaries (XB) and Planck measurements of cosmic microwave background distortions (PA). The incredulity limits (IL) correspond to one primordial black hole (PBH) per relevant environment (galaxy, cluster, Universe). There are four mass windows (A, B, C, D) in which PBHs could have an appreciable density. Possible constraints in window D are discussed in Section 6 but not in the past literature. Figure adapted from Reference 20.

the search for particle dark matter, in which there is also a split between groups searching for light and heavy candidates.

It should be stressed that nonevaporating PBHs are dark even if they do not provide all the dark matter, so this review does not focus exclusively on the proposal that PBHs solve the dark matter problem. Many objects are dark, and it is not implausible that the dark matter might comprise some mixture of PBHs and weakly interacting massive particles (WIMPs). Indeed, such a mixture would have interesting consequences for both. Also, even if PBHs provide only a small fraction of the dark matter, they may still be of great cosmological interest. For example, they could play a role in generating the SMBHs in galactic nuclei, which have obvious astrophysical significance even though they provide only 0.1% of the dark matter.

The constraints shown in **Figure 1** assume that the PBH mass function is monochromatic (i.e., width $\Delta M \sim M$). However, there are many scenarios in which one would expect the mass function to be extended. For example, inflation often produces a log-normal mass function (24),

Annu. Rev. Nucl. Part. Sci. 2020.70:355-394. Downloaded from www.annualreviews.org
Access provided by WIB6263 - Deutsches Elektronen Synchroton (DESY) on 04/08/21. See copyright for approved use.

and critical collapse generates an extended low-mass tail (25). In the context of the dark matter problem, this situation is a two-edged sword. On the one hand, it means that the total PBH density may suffice to explain the dark matter even if the density in any particular mass band is small and within the observational bounds. On the other hand, even if PBHs can provide all the dark matter at some mass scale, the extended mass function may still violate the constraints at some other scale (26). While there is now a well-understood procedure for analyzing constraints in the extended case (27), identifying the optimal PBH mass window remains problematic (28).

The proposal that the dark matter could comprise PBHs in the intermediate mass range has attracted much attention recently as a result of the LIGO/Virgo detections of merging binary black holes with mass in the range of 10 to $50M_\odot$ (29). Because the black holes are larger than initially expected, they have been suggested to represent a new population, although the mainstream view remains that they are the remnants of ordinary stars (30). One possibility is that they were of Population III origin (i.e., forming between decoupling and galaxy formation). Indeed, the suggestion that LIGO might detect gravitational waves (GWs) from coalescing intermediate-mass Population III black holes was first made more than 30 years ago (31), and, rather remarkably, Kinugawa et al. (32) predicted a Population III coalescence peak at $30M_\odot$ shortly before the first LIGO detection of black holes of that mass. Another possibility, which is more relevant to the present considerations, is that the LIGO/Virgo black holes are primordial, as first discussed in Reference 33. However, this scenario does not require the PBHs to provide all the dark matter. While this possibility has been suggested (34), the predicted merger rate depends on when the binaries form and uncertain astrophysical factors, so the dark matter fraction could still be small (35). Indeed, the LIGO/Virgo results have already been used to constrain the PBH dark matter fraction (36), although the limit is sensitive to the predicted merger rate, which is very model dependent (37). Note that the PBH density should peak at a lower mass than the coalescence signal for an extended PBH mass function because the GW amplitude scales as the black hole mass.

In Section 2 of this review, we elaborate on several aspects of PBH formation, including a general discussion of their mass and density, a review of PBH formation scenarios, and a consideration of the effects of non-Gaussianity and nonsphericity. In Section 3, we review current constraints on the density of PBHs with a monochromatic mass function, these constraints being associated with a variety of lensing, dynamical, accretion, and GW effects. At first sight, these effects seem to exclude the possibility of PBHs providing the dark matter in any mass range, but this conclusion may be avoided for an extended mass function, and most limits are subject to caveats anyway. More positively, in Section 4 we provide an overview of various observational conundra that can be explained by PBHs—especially those associated with intermediate-mass black holes and SMBHs. In Section 5, we discuss how the thermal history of the Universe naturally provides peaks in the PBH mass function at the mass scales associated with these conundra, with the bumpy mass function obviating some of the limits discussed in Section 3. We also present a recently developed mechanism that helps to resolve a long-standing fine-tuning problem associated with PBH formation. In Section 6, we discuss scenarios that involve a mixture of PBHs and particle dark matter. In Section 7, we draw some general conclusions about PBHs as dark matter.

2. PRIMORDIAL BLACK HOLE FORMATION

PBHs may have been produced during the early Universe through various mechanisms. For all such mechanisms, the increased cosmological energy density at early times plays a major role (38), yielding a rough connection between the PBH mass and the horizon mass at formation:

$$M \sim \frac{c^3 t}{G} \sim 10^{15} \left(\frac{t}{10^{-23}\,\mathrm{s}} \right) \mathrm{g}. \qquad 1.$$

Annu. Rev. Nucl. Part. Sci. 2020.70:355-394. Downloaded from www.annualreviews.org
Access provided by WIB6263 - Deutsches Elektronen Synchroton (DESY) on 04/08/21. See copyright for approved use.

Hence, PBHs could span an enormous mass range: Those formed at the Planck time (10^{-43} s) would have the Planck mass (10^{-5} g), whereas those formed at 1 s would be as large as $10^5 M_\odot$—comparable to the mass of the holes thought to reside in galactic nuclei. By contrast, black holes forming at the present epoch (e.g., in the final stages of stellar evolution) could never be smaller than about $1M_\odot$. In some circumstances, PBHs may form over an extended period, resulting in a wide range of masses. Even if they formed at a single epoch, their mass spectrum could still extend considerably below the horizon mass because of so-called critical phenomena (39–43), although most of the PBH density would still be in the most massive ones.

2.1. Mass and Density Fraction of Primordial Black Holes

The fraction of the mass of the Universe in PBHs on some mass scale M is epoch dependent, but its value at the formation epoch of the PBHs is denoted by $\beta(M)$. For the standard ΛCDM model, in which the age of the Universe is $t_0 = 13.8$ Gyr, the Hubble parameter is $h = 0.68$ (44) and the time of photon decoupling is $t_{\rm dec} = 380$ kyr (45). If the PBHs have a monochromatic mass function, the fraction of the Universe's mass in PBHs at their formation time t_i is related to their number density $n_{\rm PBH}(t_i)$ by (3)

$$\beta(M) \equiv \frac{M\, n_{\rm PBH}(t_i)}{\rho(t_i)} \approx 7.98 \times 10^{-29}\, \gamma^{-1/2} \left(\frac{g_{*i}}{106.75}\right)^{1/4} \left(\frac{M}{M_\odot}\right)^{3/2} \left(\frac{n_{\rm PBH}(t_0)}{1\,{\rm Gpc}^{-3}}\right), \qquad 2.$$

where $\rho(t_i)$ is the density at time t_i, and γ is the ratio of the PBH mass to the horizon mass. g_{*i} is the number of relativistic degrees of freedom at PBH formation, normalized to its value at 10^{-5} s because it does not increase much before that in the Standard Model, and this is the period in which most PBHs are likely to form.

The current density parameter for PBHs that have not yet evaporated is

$$\Omega_{\rm PBH} = \frac{M\, n_{\rm PBH}(t_0)}{\rho_{\rm crit}} \approx \left(\frac{\beta(M)}{1.03 \times 10^{-8}}\right)\left(\frac{h}{0.68}\right)^{-2} \gamma^{1/2} \left(\frac{g_{*i}}{106.75}\right)^{-1/4} \left(\frac{M}{M_\odot}\right)^{-1/2}, \qquad 3.$$

where $\rho_{\rm crit}$ is critical density. Equation 3 can be expressed in terms of the ratio of the current PBH mass density to the CDM density:

$$f \equiv \frac{\Omega_{\rm PBH}}{\Omega_{\rm CDM}} \approx 3.8\, \Omega_{\rm PBH} \approx 2.4\, \beta_{\rm eq}, \qquad 4.$$

where $\beta_{\rm eq}$ is the PBH mass fraction at matter–radiation equality, and we use the most recent value $\Omega_{\rm CDM} = 0.26$ indicated by the Planck Collaboration (46). The ratio of the energy densities of matter and radiation (all relativistic species) at any time is

$$\frac{\Omega_{\rm M}}{\Omega_{\rm R}} = \frac{\Omega_B + \Omega_{\rm CDM}}{\Omega_{\rm R}} \approx \frac{1700}{g_*(z)} \frac{1+\chi}{1+z}, \qquad 5.$$

where $\chi \equiv \Omega_{\rm CDM}/\Omega_B \approx 5$ is the ratio of the dark matter and baryonic densities. At PBH formation, the fraction of domains that collapse is

$$\beta \equiv f_{\rm PBH} \frac{\chi\, \Omega_B}{\Omega_{\rm R}} \simeq f_{\rm PBH} \frac{\chi\, \eta}{g_*(T)} \frac{0.7\,{\rm GeV}}{T}, \qquad 6.$$

where $\eta = n_B/n_\gamma = 6 \times 10^{-10}$ is the observed baryon-to-photon ratio (i.e., the baryon asymmetry prior to 10^{-5} s). As discussed in Section 5, this relationship suggests a scenario in which baryogenesis is linked with PBH formation, and the smallness of the η reflects the rarity of the Hubble domains that collapse (47). The collapse fraction can also be expressed as

$$\beta \approx 0.5\, f_{\rm tot} \left[\chi\, \gamma^{-1/2}\, \eta\, g_*^{1/4}\right] \left(\frac{M}{M_\odot}\right)^{1/2}, \qquad 7.$$

Annu. Rev. Nucl. Part. Sci. 2020.70:355-394. Downloaded from www.annualreviews.org
Access provided by WIB6263 - Deutsches Elektronen Synchroton (DESY) on 04/08/21. See copyright for approved use.

where $f_{\rm tot}$ is the total dark matter fraction, and the square-bracketed term has a value of order 10^{-9}.

2.2. Formation Scenarios

We now review the large number of scenarios that have been proposed for PBH formation and the associated PBH mass functions. We have seen that PBHs generally have a mass of the order of the horizon mass at formation, so one might expect a monochromatic mass function (i.e., width $\Delta M \sim M$). However, in some scenarios PBHs form over a prolonged period and therefore have an extended mass function (e.g., with its form of the mass function depending on the power spectrum of the primordial fluctuations). As discussed below, even PBHs formed at a single epoch may have an extended mass function.

2.2.1. Primordial inhomogeneities. The most natural possibility is that PBHs form from primordial density fluctuations. Overdense regions will then stop expanding sometime after they enter the particle horizon and collapse against the pressure if they are larger than the Jeans mass. If the horizon-scale fluctuations have a Gaussian distribution with dispersion σ, the fraction of horizon patches collapsing to a black hole should be (48)

$$\beta \approx \mathrm{Erfc}\left[\frac{\delta_{\rm c}}{\sqrt{2}\,\sigma}\right]. \qquad 8.$$

Here, Erfc is the complementary error function, and $\delta_{\rm c}$ is the density-contrast threshold for PBH formation. In a radiation-dominated era, a simple analytic argument (48) suggests $\delta_{\rm c} \approx 1/3$, but more precise numerical (40) and analytical (49) investigations suggest $\delta_{\rm c} = 0.45$. It should be noted that there is a distinction between the threshold value for the density and curvature fluctuation (50), and a good analytic understanding of these issues has been achieved (51). The threshold is also sensitive to any non-Gaussianity (52), the shape of the perturbation profile (53), and the equation of state of the medium (a feature exploited in Reference 54).

2.2.2. Collapse from scale-invariant fluctuations. If the PBHs form from scale-invariant fluctuations (i.e., with constant amplitude at the horizon epoch), their mass spectrum should have the following power-law form (48):

$$\frac{\mathrm{d}n}{\mathrm{d}M} \propto M^{-\alpha} \quad \text{with} \quad \alpha = \frac{2\,(1+2\,w)}{1+w}, \qquad 9.$$

where γ specifies the equation of state ($p = w\,\rho\,c^2$) at PBH formation. The exponent arises because the background density and PBH density have different redshift dependencies. At one time it was argued that the primordial fluctuations would be expected to be scale invariant (55), but this argument does not apply in the inflationary scenario. Nevertheless, the above equations should still apply if the PBHs form from cosmic loops because the collapse probability is then scale invariant. If the PBHs contain a fraction $f_{\rm DM}$ of the dark matter, then the fraction of the dark matter in PBHs with masses larger than M should be

$$f(M) \approx f_{\rm DM}\left(\frac{M_{\rm DM}}{M}\right)^{\alpha-2} \quad (M_{\rm min} < M < M_{\rm max}), \qquad 10.$$

where $2 < \alpha < 3$, and $M_{\rm DM} \approx M_{\rm min}$ is the mass scale that contains most of the dark matter. In a radiation-dominated era, the exponent in Equation 10 becomes 1/2.

Annu. Rev. Nucl. Part. Sci. 2020.70:355-394. Downloaded from www.annualreviews.org
Access provided by WIB6263 - Deutsches Elektronen Synchroton (DESY) on 04/08/21. See copyright for approved use.

Annu. Rev. Nucl. Part. Sci. 2020.70:355-394. Downloaded from www.annualreviews.org
Access provided by WIB6263 - Deutsches Elektronen Synchroton (DESY) on 04/08/21. See copyright for approved use.

2.2.3. Collapse in a matter-dominated era. PBHs form more easily if the Universe becomes pressureless (i.e., matter-dominated) for some period. For example, this scenario may arise at a phase transition in which the mass is channeled into nonrelativistic particles (56) or because of slow reheating after inflation (57, 58). In a related context, Hidalgo et al. (59) have recently studied PBH formation in a dust-like scenario of an oscillating scalar field during an extended period of preheating. Because the value of α in the above analysis is 2 for $\gamma = 0$, one might expect $\rho(M)$ to increase logarithmically with M. However, the analysis breaks down in this case because the Jeans length is much smaller than the particle horizon, so pressure is not the main inhibitor of collapse. Instead, collapse is prevented by deviations from spherical symmetry, and the probability of PBH formation can be shown to be (56)

$$\beta(M) = 0.02\,\delta_{\rm H}(M)^5. \qquad 11.$$

This approach is consistent with the recent analysis of Harada et al. (60) and leads to a mass function

$$\frac{{\rm d}n}{{\rm d}M} \propto M^{-2}\,\delta_{\rm H}(M)^5. \qquad 12.$$

The collapse fraction $\beta(M)$ is still small for $\delta_{\rm H}(M) \ll 1$ but is much larger than the exponentially suppressed fraction in the radiation-dominated case. If the matter-dominated phase extends from t_1 to t_2, PBH formation is enhanced over the mass range

$$M_{\rm min} \sim M_{\rm H}(t_1) < M < M_{\rm max} \sim M_{\rm H}(t_2)\,\delta_{\rm H}(M_{\rm max})^{3/2}. \qquad 13.$$

The lower limit is the horizon mass at the start of matter dominance, and the upper limit is the horizon mass when the regions that bind at the end of matter dominance enter the horizon. This scenario has recently been studied in Reference 61.

2.2.4. Collapse from inflationary fluctuations. If the fluctuations generated by inflation have a blue spectrum (i.e., decrease with increasing scale) and the PBHs form from the high-σ tail of the fluctuation distribution, then the exponential factor in Equation 8 might suggest that the PBH mass function should have an exponential upper cutoff at the horizon mass when inflation ends. This epoch corresponds to the reheat time $t_{\rm R}$, which the cosmic microwave background (CMB) quadrupole anisotropy requires to exceed 10^{-35} s, so this argument places a lower limit of around 1 g on the masses of such PBHs. The first inflationary scenarios for PBH formation were proposed in Reference 62, and subsequently there have been many papers on this topic. In some scenarios, the PBHs form from a smooth symmetric peak in the inflationary power spectrum, in which case the PBH mass function should have the following log-normal form:

$$\frac{{\rm d}n}{{\rm d}M} \propto \frac{1}{M^2}\,\exp\left[-\frac{(\log M - \log M_{\rm c})^2}{2\,\sigma^2}\right]. \qquad 14.$$

This form was first suggested by Dolgov & Silk (24) (see also References 22 and 63) and has been demonstrated both numerically (26) and analytically (64) for cases in which the slow-roll approximation holds. It is therefore representative of a large class of inflationary scenarios, including the axion-like curvaton and running-mass inflation models considered by Kühnel et al. (43). Equation 14 implies that the mass function is symmetric about its peak at $M_{\rm c}$ and described by two parameters: the mass scale $M_{\rm c}$ itself and the width of the distribution σ. The integrated mass function is

$$f(M) = \int_M {\rm d}\tilde{M}\,\tilde{M}\,\frac{{\rm d}n}{{\rm d}\tilde{M}} \approx {\rm Erfc}\left(\ln\frac{M}{\sigma}\right). \qquad 15.$$

However, not all inflationary scenarios produce the mass function given by Equation 14. Inomata et al. (65) propose a scenario that combines a broad mass function at low M (to explain the dark matter) with a sharp one at high m (to explain the LIGO events).

2.2.5. Quantum diffusion. Most of the relevant inflationary dynamics happens in regimes in which the classical inflaton-field evolution dominates over the field's quantum fluctuations. Under certain circumstances, however, the situation is reversed. There are two cases in which this happens. The first applies when the inflaton assumes larger values of its potential $V(\varphi)$, yielding eternally expanding patches of the Universe (66). The second applies when the inflaton potential possesses one or more plateau-like features. Classically, using the slow-roll conditions $|\ddot{\varphi}| \ll 3\,H\,|\dot{\varphi}|$ and $(\dot{\varphi})^2 \ll 2\,V(\varphi)$ (where an overdot represents a derivative with regard to cosmic time t, $H \equiv \dot{a}/a$ is the Hubble parameter, and a is the scale factor), the number of inflationary e-folds is $N = \int \mathrm{d}\varphi\; H/\dot{\varphi}$, which implies $\delta\varphi_\mathrm{C} = \dot{\varphi}/H$. On the other hand, the corresponding quantum fluctuations are $\delta\varphi_\mathrm{Q} = H/2\pi$. Because the primordial metric perturbation is

$$\zeta = \frac{H}{\dot{\varphi}}\,\delta\varphi = \frac{\delta\varphi_\mathrm{Q}}{\delta\varphi_\mathrm{C}}, \qquad 16.$$

quantum effects are expected to be important whenever this quantity becomes of order one—that is, $\zeta \sim \mathcal{O}(1)$. This is often the case for PBH formation, for which recent investigations indicate an increase of the power spectrum and hence the PBH abundance (67). This quantum diffusion is inherently nonperturbative; thus, Kühnel & Freese (68) have developed a dedicated resummation technique to incorporate all higher-order corrections (for an application of these techniques to stochastic inflation, see Reference 69). Ezquiaga et al. (70) have argued that quantum diffusion generically generates a high degree of non-Gaussianity.

2.2.6. Critical collapse. It is well known that black hole formation is associated with critical phenomena (71), and various authors have applied this feature in investigations of PBH formation (42, 43, 72, 73). The conclusion is that the mass function has an upper cutoff at around the horizon mass, but there is also a low-mass tail (74). If we assume for simplicity that the density fluctuations have a monochromatic power spectrum on some mass scale K and identify the amplitude of the density fluctuation when that scale crosses the horizon, δ, as the control parameter, then the black hole mass is (71)

$$M = K\left(\delta - \delta_\mathrm{c}\right)^{\eta}. \qquad 17.$$

Here, K can be identified with a mass M_f of the order of the particle horizon mass, δ_c is the critical fluctuation required for PBH formation, and the exponent η has a universal value for a given equation of state. For $\gamma = 1/3$, one has $\delta_\mathrm{c} \approx 0.4$ and $\eta \approx 0.35$. Although the scaling relation shown by Equation 17 is expected to be valid only in the immediate neighborhood of δ_c, most black holes should form from fluctuations with this value because the probability distribution function declines exponentially beyond $\delta = \delta_\mathrm{c}$ if the fluctuations are blue. Hence, it is sensible to calculate the expected PBH mass function using Equation 17. This allows us to estimate the mass function independently of the form of the probability distribution function of the primordial density fluctuations. A detailed calculation gives the following mass function (25):

$$\frac{\mathrm{d}n}{\mathrm{d}M} \propto \left(\frac{M}{\xi\,M_\mathrm{f}}\right)^{1/\eta-1} \exp\left[-(1-\eta)\left(\frac{M}{\eta\,M_\mathrm{f}}\right)^{1/\eta}\right], \qquad 18.$$

where $\xi \equiv (1-\eta/s)^{\eta}$, $s = \delta_\mathrm{c}/\sigma$, $M_\mathrm{f} = K$, and σ is the dispersion of δ. The above analysis depends on the assumption that the power spectrum of the primordial fluctuations is monochromatic. As

Annu. Rev. Nucl. Part. Sci. 2020.70:355-394. Downloaded from www.annualreviews.org
Access provided by WIB6263 - Deutsches Elektronen Synchroton (DESY) on 04/08/21. See copyright for approved use.

shown by Kühnel et al. (43) for a variety of inflationary models, when a realistic model for the power spectrum is used, the inclusion of critical collapse can lead to a significant shift, lowering and broadening the PBH mass spectra—in some cases by several orders of magnitude.

2.2.7. Collapse at QCD phase transition. At one stage it was thought that the QCD phase transition at 10^{-5} s might be first order, which would mean that the quark–gluon plasma and hadron phases could coexist: The cosmic expansion would proceed at constant temperature by converting the quark–gluon plasma to hadrons. The sound-speed would then vanish and the effective pressure would be reduced, significantly lowering the threshold δ_c for collapse. PBH production during a first-order QCD phase transition was first suggested by Crawford & Schramm (75) and later revisited by Jedamzik (76). The amplification of density perturbations due to the vanishing of the speed of sound during the QCD transition was also considered by Schmid and colleagues (77), while Caldwell & Casper (78) developed a semianalytic approach for PBH production during the transition. It is now thought unlikely that the QCD transition is first order, but one still expects some softening in the equation of state. Recently, Byrnes et al. (23) have discussed how this softening—when combined with critical phenomena and the exponential sensitivity of $\beta(M)$ to the equation of state—could produce a significant change in the mass function. The mass of a PBH forming at the QCD epoch is

$$M = \frac{\gamma\,\xi^2}{g_*^{1/2}}\left(\frac{45}{16\pi^3}\right)^{1/2}\frac{M_{\rm Pl}^3}{m_p^2} \approx 0.9\left(\frac{\gamma}{0.2}\right)\left(\frac{g_*}{10}\right)^{-1/2}\left(\frac{\xi}{5}\right)^2 M_\odot, \qquad 19.$$

where $M_{\rm Pl}$ is the Planck mass, m_p is the proton mass, g_* is normalized appropriately, and $\xi \equiv m_p/(k_{\rm B}\,T) \approx 5$ is the ratio of the proton mass to the QCD transition temperature. This PBH mass is necessarily close to the Chandrasekhar mass:

$$M_{\rm Ch} = \frac{\omega}{\tilde{\mu}^2}\left(\frac{3\pi}{4}\right)^{1/2}\frac{M_{\rm Pl}^3}{m_p^2} \simeq 5.6\,\tilde{\mu}^{-2}\,M_\odot, \qquad 20.$$

where $\omega = 2.018$ is a constant that appears in the solution of the Lane-Emden equation, and $\tilde{\mu}$ is the number of electrons per nucleon (one for hydrogen, two for helium). The two masses are very close for the relevant parameter choices. Because all stars have a mass in the range (0.1–10) $M_{\rm Ch}$, an interesting consequence is that dark and visible objects have comparable masses. From Equation 7, it is also interesting that the collapse fraction at the QCD epoch is

$$\beta \approx 0.4\,f^{\rm tot}\,\chi\,\eta\,\xi \approx 10\,\eta, \qquad 21.$$

where we have assumed $f^{\rm tot} \approx 1$ and $\chi \approx 5.5$ at the last step. This result is easily understood since one necessarily has $\rho_B/\rho_\gamma \sim \eta$ at the QCD epoch. We exploit this result in Section 5 by suggesting that the collapse fraction determines the baryon asymmetry.

2.2.8. Collapse of cosmic loops. In the cosmic string scenario, one expects some strings to self-intersect and form cosmic loops. A typical loop will be larger than its Schwarzschild radius by the factor $(G\,\mu)^{-1}$, where μ is the string mass per unit length. If strings play a role in generating large-scale structure, $G\,\mu$ must be of order 10^{-6}. However, as discussed by many authors (79, 80), there is always a small probability that a cosmic loop will get into a configuration in which every dimension lies within its Schwarzschild radius. This probability depends on both μ and the string correlation scale. The holes form with equal probability at every epoch, so they should have an extended mass spectrum with (79)

$$\beta \sim (G\,\mu)^{2x-4}, \qquad 22.$$

Annu. Rev. Nucl. Part. Sci. 2020.70:355-394. Downloaded from www.annualreviews.org
Access provided by WIB6263 - Deutsches Elektronen Synchroton (DESY) on 04/08/21. See copyright for approved use.

where $x \equiv L/s$ is the ratio of the string length to the correlation scale. One expects $2 < x < 4$ and requires $G\mu < 10^{-7}$ to avoid overproduction of PBHs.

2.2.9. Collapse through bubble collisions. Bubbles of broken symmetry might arise at any spontaneously broken symmetry epoch, and various authors have suggested that PBHs could form as a result of bubble collisions (75, 81). However, this result occurs only if the bubble formation rate per Hubble volume is finely tuned: If it is much larger than the Hubble rate, the entire Universe undergoes the phase transition immediately, and there is not time to form black holes; if it is much less than the Hubble rate, the bubbles are very rare and never collide. The holes should have a mass on the order of the horizon mass at the phase transition, so PBHs forming at the grand unification epoch would have a mass of 10^3 g, those forming at the electroweak unification epoch would have a mass of 10^{28} g, and those forming at the QCD (quark–hadron) phase transition would have a mass of around $1M_\odot$. There could also be wormhole production at a first-order phase transition (82). The production of PBHs from bubble collisions at the end of first-order inflation has been studied extensively by Khlopov and colleagues (83).

2.2.10. Collapse of domain walls. The collapse of sufficiently large closed domain walls produced at a second-order phase transition in the vacuum state of a scalar field, such as might be associated with inflation, could lead to PBH formation (84). These PBHs would have a small mass for a thermal phase transition with the usual equilibrium conditions. However, they could be much larger in a nonequilibrium scenario (85). Indeed, these PBHs could span a wide range of masses with a fractal structure of smaller PBHs clustered around larger ones (83). Vilenkin and colleagues (86) have argued that bubbles formed during inflation would (depending on their size) form either black holes or baby universes connected to our Universe by wormholes. In this case, the PBH mass function would be very broad and extend to very high masses (87).

2.3. Non-Gaussianity and Nonsphericity

As PBHs form from the high-density tail of the spectrum of fluctuations, their abundance is acutely sensitive to non-Gaussianities in the density perturbation profile (88). For certain models—such as the hybrid waterfall or simple curvaton models (89)—it even has been shown that no truncation of non-Gaussian parameters can be made to the model without changing the estimated PBH abundance (88). However, non-Gaussianity-induced PBH production can have serious consequences for the viability of PBH dark matter. PBHs produced with non-Gaussianity lead to isocurvature modes that could be detected in the CMB (90). With the current Planck exclusion limits (44), this argument implies that the non-Gaussianity parameters $f_{\rm NL}$ and $g_{\rm NL}$ for a PBH-producing theory are both less than $\mathcal{O}(10^{-3})$. For theories like the curvaton and hybrid inflation models (22, 91), this leads to the immediate exclusion of PBH dark matter because the isocurvature effects would be too large.

Nonsphericity has not yet been subject to extensive numerical studies of the kind described in Reference 40, but nonzero ellipticity leads to possibly large effects on the PBH mass spectra. Reference 53 gives an approximate analytical approximation for the collapse threshold, which will be larger than in the spherical case,

$$\delta_{\rm ec}/\delta_{\rm c} \simeq 1 + \kappa \left(\frac{\sigma^2}{\delta_{\rm c}^2}\right)^{\tilde{\gamma}}, \qquad 23.$$

where $\delta_{\rm c}$ is the threshold value for spherical collapse, σ^2 is the amplitude of the density power spectrum at the given scale, $\kappa = 9/\sqrt{10\pi}$, and $\tilde{\gamma} = 1/2$. Although Reference 92 had already

Annu. Rev. Nucl. Part. Sci. 2020.70:355-394. Downloaded from www.annualreviews.org
Access provided by WIB6263 - Deutsches Elektronen Synchroton (DESY) on 04/08/21. See copyright for approved use.

obtained this result for a limited class of cosmologies, it did not include the case of ellipsoidal collapse in a radiation-dominated model. A thorough numerical investigation is still needed to precisely determine the change of the threshold for fully relativistic nonspherical collapse. It also should be noted that the effect due to nonsphericities is partly degenerate with that of non-Gaussianities (53).

2.4. Multispike Mass Functions

If PBHs are to explain phenomena on different mass scales, it is pertinent to consider the possibility that the PBH mass spectrum might have several spikes. There are two known recent mechanisms for generating such spikes. The first has been proposed by Cai et al. (93), who discuss a new type of resonance effect that leads to prolific PBH formation. This effect arises because the sound-speed can oscillate in some inflationary scenarios, leading to parametric amplification of the curvature perturbation and hence a significant peak in the power spectrum of the density perturbations on some critical scale. The resonances are in narrow bands around certain harmonic frequencies with one of the peaks dominating. It turns out that one can easily get a peak of order unity. Although most PBHs form at the first peak, a small number will also form at subsequent peaks. The second mechanism for generating multispiked PBH mass spectra, as recently proposed by Carr & Kühnel (94), has been demonstrated for most of the well-studied models of PBH formation. This mechanism relies on the choice of non-Bunch-Davies vacua, leading to oscillatory features in the inflationary power spectrum, which in turn generate oscillations in the PBH mass function with exponentially enhanced spikes.

3. CONSTRAINTS AND CAVEATS

In this section, we review the various constraints for PBHs that are too large to have evaporated completely by now (we update the equivalent discussions from References 3 and 13). All the limits assume that PBHs cluster in the Galactic halo in the same way as do other forms of CDM unless they are so large that there is less than one per galaxy. Throughout this section, the PBHs are taken to have a monochromatic mass function in that they span a mass range $\Delta M \sim M$. In this case, the fraction $f(M)$ of the halo in PBHs is related to $\beta(M)$ by Equation 3. Our limits on $f(M)$ are summarized in **Figure 1**, which is based on figure 10 of Reference 20 (which provides a much more comprehensive review of the PBH constraints). Following Reference 95, the constraints are also broken down according to the redshift of the relevant observations sketched in **Figure 2**. The main constraints derive from PBH evaporations, various gravitational-lensing experiments, numerous dynamical effects, and PBH accretion. Where there are several limits in the same mass range, we usually show only the most stringent one. It must be stressed that the constraints in **Figures 1** and **2** have varying degrees of certainty, and they all come with caveats. For some, the observations are well understood but there are uncertainties in the black hole physics. For others, the observations themselves are not fully understood or depend on additional astrophysical assumptions. The constraints may also depend on other physical parameters that are not shown explicitly. It is important to stress that some of the constraints can be circumvented if the PBHs have an extended mass function. Indeed, as discussed in Section 5, an extended mass function may be required if PBHs are to provide most of the dark matter.

3.1. Evaporation Constraints

A PBH of initial mass M will evaporate through the emission of Hawking radiation on a timescale $\tau \propto M^3$, which is less than the present age of the Universe for M below $M_* \approx 5 \times 10^{14}$ g (97).

Annu. Rev. Nucl. Part. Sci. 2020.70:355-394. Downloaded from www.annualreviews.org
Access provided by WIB6263 - Deutsches Elektronen Synchroton (DESY) on 04/08/21. See copyright for approved use.

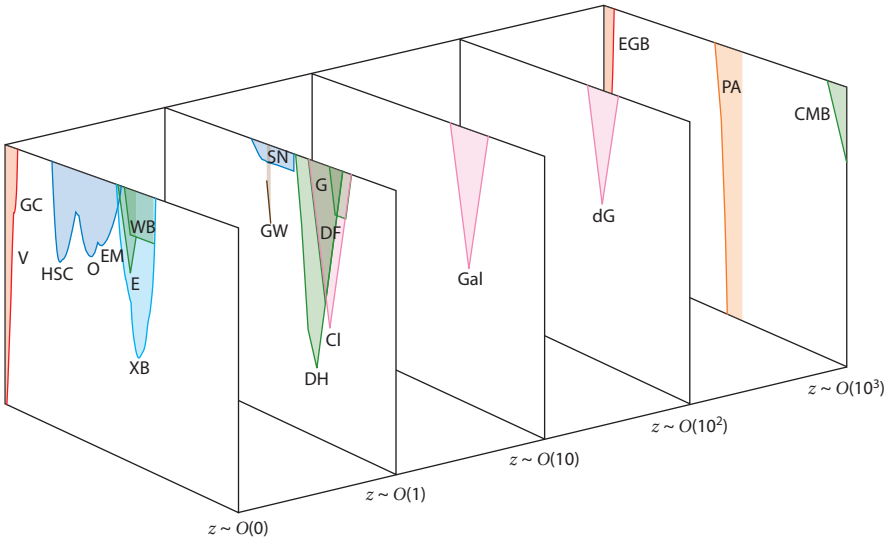

Figure 2

Sketch of the limits shown in **Figure 1** for different redshifts. The large-scale structure limit is broken down into its individual components from clusters (Cl), Milky Way galaxies (Gal), and dwarf galaxies (dG), as these components originate from different redshifts (cf. Reference 96). Abbreviations are defined in the caption to **Figure 1**.

There is a strong constraint on $f(M_*)$ from observations of the extragalactic γ-ray background (4). PBHs in the narrow band $M_* < M < 1.005M_*$ have not yet completed their evaporation, but their current mass is below the mass $M_q \approx 0.4M_*$, at which quark and gluon jets are emitted. For $M > 2M_*$, one can neglect the change of mass altogether and obtain the time-integrated spectrum of photons from each PBH by multiplying the instantaneous spectrum by the age of the Universe t_0. The instantaneous spectrum for primary (nonjet) photons is

$$\frac{\mathrm{d}\dot{N}_\gamma^{\mathrm{p}}}{\mathrm{d}E}(M, E) \propto \frac{E^2\,\sigma(M, E)}{\mathrm{e}^{EM} - 1} \propto \begin{cases} E^3\,M^3 & (E < M^{-1}) \\ E^2\,M^2\,\mathrm{e}^{-EM} & (E > M^{-1}), \end{cases} \quad 24.$$

where $\sigma(M, E)$ is the absorption cross-section for photons of energy E, so this gives an intensity

$$I(E) \propto f(M) \times \begin{cases} E^4\,M^2 & (E < M^{-1}) \\ E^3\,M\,\mathrm{e}^{-EM} & (E > M^{-1}). \end{cases} \quad 25.$$

This peaks at $E_{\max} \propto M^{-1}$ with a value $I_{\max}(M) \propto f(M)\,M^{-2}$, whereas the observed intensity is $I_{\mathrm{obs}} \propto E^{-(1+\epsilon)}$ with ϵ between 0.1 and 0.4. Therefore, putting $I_{\max}(M) < I_{\mathrm{obs}}(M(E))$ gives (3)

$$f(M) < 2 \times 10^{-8} \left(\frac{M}{M_*}\right)^{3+\epsilon} \quad (M > M_*). \quad 26.$$

We plot this constraint in **Figure 1** for $\epsilon = 0.2$. The Galactic γ-ray background constraint could give a stronger limit (97), but this depends sensitively on the form of the PBH mass function, so we do not discuss it here.

There are various other evaporation constraints in this mass range. Boudad & Cirelli (98) use positron data from Voyager 1 to constrain evaporating PBHs of mass $M < 10^{16}$ g and obtain the bound $f < 0.001$. This finding, which complements the cosmological limit as it is based on local

Annu. Rev. Nucl. Part. Sci. 2020.70:355-394. Downloaded from www.annualreviews.org
Access provided by WIB6263 - Deutsches Elektronen Synchroton (DESY) on 04/08/21. See copyright for approved use.

Galactic measurements, is also shown in **Figure 1**. Laha (99) and DeRocco & Graham (100) constrain PBHs in the mass range 10^{16}–10^{17} g using measurements of the 511-keV annihilation line radiation from the Galactic center. Other limits are associated with γ-ray and radio observations of the Galactic center (101) and the ionizing effect of PBHs in the mass range 10^{16}–10^{17} g (8).

3.2. Lensing Constraints

Constraints on massive compact halo objects (MACHOs) with very low M have been claimed from the femtolensing of γ-ray bursts. Assuming the bursts are at a redshift $z \sim 1$, early studies implied $f < 1$ in the mass range 10^{-16}–$10^{-13} M_\odot$ (102) and $f < 0.1$ in the range 10^{-17}–$10^{-14} M_\odot$ (103). However, Katz et al. (104) argue that most γ-ray burst sources are too large for these limits to apply, so we do not show them in **Figure 1**. Kepler data from observations of Galactic sources (105) imply a limit on the planetary-mass range: $f(M) < 0.3$ for $2 \times 10^{-9} M_\odot < M < 10^{-7} M_\odot$. However, Niikura et al. (106) carried out a 7-h observation of M31 with the Subaru Hyper Suprime-Cam (HSC) to search for microlensing of stars by PBHs lying in the halo regions of the Milky Way and M31; they obtained a much more stringent bound for $10^{-10} < M < 10^{-6} M_\odot$, which is shown in **Figure 1**.

Microlensing observations of stars in the Large Magellanic Cloud (LMC) and Small Magellanic Cloud (SMC) probe the fraction of the Galactic halo in MACHOs in a certain mass range (107). The optical depth of the halo toward the LMC and SMC is related to the fraction $f(M)$ by $\tau_{\rm L}^{\rm (SMC)} = 1.4\, \tau_{\rm L}^{\rm (LMC)} = 6.6 \times 10^{-7}\, f(M)$ for the standard halo model (108). The MACHO Collaboration detected lenses with $M \sim 0.5 M_\odot$ but concluded that their halo contribution could be at most 10% (109), while the EROS Collaboration excluded objects in the range $6 \times 10^{-8} M_\odot < M < 15 M_\odot$ from dominating the halo. Since then, further limits in the range $0.1 M_\odot < M < 20 M_\odot$ have come from the OGLE experiment (110). The combined results can be approximated by

$$f(M) < \begin{cases} 1 & (6 \times 10^{-8} M_\odot < M < 30 M_\odot) \\ 0.1 & (10^{-6} M_\odot < M < 1 M_\odot) \\ 0.05 & (10^{-3} M_\odot < M < 0.4 M_\odot). \end{cases} \quad 27.$$

Recently, Niikura et al. (111) have used data from a 5-year OGLE survey of the Galactic bulge to place much stronger limits in the range $10^{-6} M_\odot < M < 10^{-4} M_\odot$, although they also claim some positive detections. The precise form of the EROS and OGLE limits is shown in **Figure 1**, while the possible detections are discussed in Section 4.

PBHs cause most lines of sight to be demagnified relative to the mean, with a long tail of high magnifications. Zumalacárregui & Seljak (112) have used the lack of lensing in type Ia supernovae to constrain any PBH population, an approach that allows for the effects of large-scale structure and possible non-Gaussianity in the intrinsic supernovae luminosity distribution. Using current JLA data, they derive a bound of $f < 0.35$ for $10^{-2} M_\odot < M < 10^4 M_\odot$, with the finite size of supernovae providing the lower limit; this constraint is shown in **Figure 1**. García-Bellido et al. (113) argue that this limit can be weakened if the PBHs have an extended mass function or are clustered. There is some dispute about this claim, but **Figure 1** is only for a monochromatic mass function anyway.

The recent discovery of fast transient events in massive galaxy clusters is attributed to individual stars in giant arcs being highly magnified as a result of caustic crossing. Oguri et al. (114) argue that observations of the particular event MACS J1149 excluded a high density of PBHs anywhere in the mass range $10^{-5} M_\odot < M < 10^2 M_\odot$ because this would reduce the magnifications.

Annu. Rev. Nucl. Part. Sci. 2020.70:355-394. Downloaded from www.annualreviews.org
Access provided by WIB6263 - Deutsches Elektronen Synchroton (DESY) on 04/08/21. See copyright for approved use.

Early studies of the microlensing of quasars (115) seemed to exclude the possibility of all the dark matter being in objects with $10^{-3}M_\odot < M < 60M_\odot$, although this limit preceded the ΛCDM picture. More recent studies of quasar microlensing suggest a limit (116) of $f(M) < 1$ for $10^{-3}M_\odot < M < 60M_\odot$, although we argue in Section 4 that these surveys may also provide positive evidence for PBHs. Millilensing of compact radio sources (117) gives the following limit:

$$f(M) < \begin{cases} (M/2\times 10^4 M_\odot)^{-2} & (M < 10^5 M_\odot) \\ 0.06 & (10^5 M_\odot < M < 10^8 M_\odot) \\ (M/4\times 10^8 M_\odot)^2 & (M > 10^8 M_\odot). \end{cases} \quad 28.$$

Though it is weaker than the dynamical constraints in this mass range, and not included in **Figure 1**, we mention it because it illustrates that lensing limits extend to very large values of M.

3.3. Dynamical Constraints

The effects of collisions of planetary-mass PBHs on astronomical objects have been a subject of long-standing interest, although we do not show these constraints in **Figure 1** because they are controversial. Roncadelli et al. (118) have suggested that halo PBHs could be captured and swallowed by stars in the Galactic disc. The stars would eventually be accreted by the holes, producing radiation and a population of subsolar black holes that could only be of primordial origin, which would lead to a constraint of $f < (M/3\times 10^{26}\ \mathrm{g})$ corresponding to a lower limit on the mass. Capela et al. have constrained PBH dark matter by considering the capture of PBHs by white dwarfs (119) or neutron stars (120), while Pani & Loeb (121) argue that this approach excludes PBHs from providing the dark matter throughout the sublunar window. However, these limits have been disputed (122) because the dark matter density in globular clusters is now known to be much lower than assumed in these analyses (123). Graham et al. (124) argue that the transit of a PBH through a white dwarf causes localized heating through dynamical friction and initiates runaway thermonuclear fusion, causing the white dwarf to explode as a supernova. They claim that the shape of the observed white dwarf distribution excludes PBHs in the mass range of 10^{19}–10^{20} g from providing the dark matter and that those in the range of 10^{20}–10^{22} g are constrained by the observed supernova rate. However, these limits are inconsistent with hydrodynamical simulations by Montero-Camacho et al. (125), who conclude that this mass range is still allowed.

Various dynamical constraints come into play at higher mass scales (126). Many of them involve the destruction of astronomical objects by the passage of nearby PBHs. If the PBHs have density ρ and velocity dispersion V, while the objects have mass M_c, radius R_c, velocity dispersion V_c, and survival time t_L, then the constraint has the following form:

$$f(M) < \begin{cases} M_c V/(G M \rho\, t_L\, R_c) & [M < M_c(V/V_c)] \\ M_c/(\rho\, V_c\, t_L\, R_c^2) & [M_c(V/V_c) < M < M_c(V/V_c)^3] \\ M V_c^2/\left(\rho\, R_c^2\, V^3\, t_L\right) \exp\left[(M/M_c)(V_c/V)^3\right] & [M > M_c(V/V_c)^3]. \end{cases} \quad 29.$$

The three limits correspond to disruption by multiple encounters, one-off encounters, and non-impulsive encounters, respectively. The fraction is thus constrained over the mass range

$$\frac{M_c V}{G\,\rho_{DM}\, t_L\, R_c} < M < M_c \left(\frac{V}{V_c}\right)^3, \quad 30.$$

with the limits corresponding to the values of M for which $f = 1$. Various numerical factors are omitted in this discussion. These limits apply provided there is at least one PBH within the relevant

Annu. Rev. Nucl. Part. Sci. 2020.70:355-394. Downloaded from www.annualreviews.org
Access provided by WIB6263 - Deutsches Elektronen Synchroton (DESY) on 04/08/21. See copyright for approved use.

environment, which is termed the incredulity limit (126). For an environment of mass M_E, this limit corresponds to the condition $f(M) > (M/M_E)$, where M_E is around $10^{12}M_\odot$ for halos, $10^{14}M_\odot$ for clusters, and $10^{22}M_\odot$ for the Universe. In some contexts, the incredulity limit renders the third expression in Equation 29 irrelevant.

One can apply this argument to wide binaries in the Galaxy, which are particularly vulnerable to disruption by PBHs (127, 128). In the context of the original analysis of Reference 129, Equation 29 gives a constraint of $f(M) < (M/500M_\odot)^{-1}$ for $M < 10^3M_\odot$, with $500M_\odot$ representing the upper bound on the mass of PBHs that dominate the halo and $10^3M_\odot$ being the mass at which the limit flattens off. Only the flat part of the constraint appears in **Figure 1**. However, the upper limit has been reduced to $\sim 10M_\odot$ in later work (130), so the narrow window between the microlensing lower bound and the wide binary upper bound is shrinking. On the other hand, Tian et al. (131) have recently studied more than 4,000 halo wide binaries in the Gaia survey and detected a break in their separation distribution that may be indicative of PBHs with $M > 10M_\odot$.

A similar argument for the survival of globular clusters against tidal disruption by passing PBHs gives a limit of $f(M) < (M/3 \times 10^4M_\odot)^{-1}$ for $M < 10^6M_\odot$, although this depends sensitively on the mass and the radius of the cluster (126). The upper limit of $3 \times 10^4M_\odot$ is consistent with the numerical calculations of Moore (132). In a related argument, Brandt (133) infers an upper limit of $5M_\odot$ from the fact that a star cluster near the center of the dwarf galaxy Eridanus II has not been disrupted by halo objects. Koushiappas & Loeb (134) have also studied the effects of black holes on the dynamical evolution of dwarf galaxies. They find that mass segregation leads to a depletion of stars in the centers of such galaxies and the appearance of a ring in the projected stellar surface density profile. Using Segue 1 as an example, they exclude the possibility of more than 4% of the dark matter being PBHs of around $10M_\odot$. One would also expect sufficiently large PBHs to disrupt ultrafaint dwarf galaxies (UFDGs), and a recent study of 27 UFDGs by Stegmann et al. (135) appears to exclude PBHs in the mass range $1–100M_\odot$ from providing the dark matter. Only the Eridanus limit is shown in **Figure 1**.

Halo objects will overheat the stars in the Galactic disc unless $f(M) < (M/3 \times 10^6M_\odot)^{-1}$ for $M < 3 \times 10^9M_\odot$ (136). The incredulity limit, $f(M) < (M/10^{12}M_\odot)$ (corresponding to one PBH per halo), takes over for $M > 3 \times 10^9M_\odot$, and this is the only part of the limit that appears in **Figure 1**. Another limit in this mass range arises because halo objects will be dragged into the nucleus of the Galaxy by the dynamical friction of various stellar populations, and this process leads to excessive nuclear mass unless $f(M)$ is constrained (126). As shown in **Figure 1**, this limit has a complicated form because there are different sources of friction, and it also depends on parameters such as the halo core radius, but it bottoms out at $M \sim 10^7M_\odot$ with a value $f \sim 10^{-5}$.

There are also interesting limits for black holes that are too large to reside in galactic halos. The survival of galaxies in clusters against tidal disruption by giant cluster PBHs gives a limit of $f(M) < (M/7 \times 10^9M_\odot)^{-1}$ for $M < 10^{11}M_\odot$, with the limit flattening off for $10^{11}M_\odot < M < 10^{13}M_\odot$ and then rising as $f(M) < M/10^{14}M_\odot$ because of the incredulity limit. This constraint is shown in **Figure 1** with typical values for the mass and the radius of the cluster. If there were a population of huge intergalactic PBHs with density parameter $\Omega_{IG}(M)$, each galaxy would have a peculiar velocity due to its gravitational interaction with the nearest one (137). The typical distance to the nearest PBH should be $d \approx 30\,\Omega_{IG}(M)^{-1/3}(M/10^{16}M_\odot)^{1/3}$ Mpc, which should induce a peculiar velocity $V_{pec} \approx GMt_0/d^2$ over the age of the Universe. Since the CMB dipole anisotropy shows that the peculiar velocity of our Galaxy is only 400 km s^{-1}, one infers $\Omega_{IG} < (M/5 \times 10^{15}M_\odot)^{-1/2}$, which gives the limit on the far right-hand side of **Figure 1**. This limit intersects the incredulity limit (corresponding to one PBH within the particle horizon) at $M \sim 10^{21}M_\odot$.

Carr & Silk (96) point out that large PBHs could generate cosmic structures through the seed or Poisson effect even if f is small. If a region of mass $\mathcal{M}$ contains PBHs of mass M, the initial

Annu. Rev. Nucl. Part. Sci. 2020.70:355-394. Downloaded from www.annualreviews.org
Access provided by WIB6263 - Deutsches Elektronen Synchroton (DESY) on 04/08/21. See copyright for approved use.

fluctuation is $M/\mathcal{M}$ for the seed effect and $(fM/\mathcal{M})^{1/2}$ for the Poisson effect, with the fluctuation growing as z^{-1} from the redshift of CDM domination ($z_{\rm eq} \approx 4{,}000$). Even if PBHs do not play a role in generating cosmic structures, one can place interesting upper limits on the fraction of dark matter in them by requiring that various types of structure do not form too early. For example, if we apply this argument to Milky Way–type galaxies, assuming that these have a typical mass of $10^{12} M_\odot$ and must not bind before a redshift $z_B \sim 3$, we obtain

$$f(M) < \begin{cases} (M/10^6 M_\odot)^{-1} & (10^6 M_\odot < M \lesssim 10^9 M_\odot) \\ M/10^{12} M_\odot & (10^9 M_\odot \lesssim M < 10^{12} M_\odot), \end{cases} \quad 31.$$

with the second expression corresponding to having one PBH per galaxy. This limit bottoms out at $M \sim 10^9 M_\odot$ with a value $f \sim 10^{-3}$. Similar constraints apply for the first bound clouds, dwarf galaxies, and clusters of galaxies, and the limits for all the systems are collected together in **Figure 1**. The Poisson effect also influences the distribution of the Lyman-α forest (138); the associated PBH constraint has a similar form to Equation 31 but could be much stronger, with the lower limit of $10^6 M_\odot$ reduced to around $10^2 M_\odot$.

3.4. Accretion Constraints

PBHs could have a large luminosity at early times because of the accretion of background gas, and this effect imposes strong constraints on their number density. However, the analysis of the problem is complicated because the black hole luminosity will generally boost the matter temperature of the background Universe well above the standard Friedmann value even if the PBH density is small, thereby reducing the accretion. Thus, there are two distinct but related PBH constraints: one associated with the effects on the Universe's thermal history and the other with the generation of background radiation.

This problem was first studied in Reference 12, and we briefly review that analysis here. Even though this study was incomplete and later superseded by more detailed numerical investigations, we discuss it because it is the only analysis that applies for very large PBHs. Reference 12 assumes that each PBH accretes at the Bondi rate (139)

$$\dot{M} \approx 10^{11} (M/M_\odot)^2 \left(n/{\rm cm}^{-3}\right) \left(T/10^4\,{\rm K}\right)^{-3/2} {\rm g\,s}^{-1}, \quad 32.$$

where a dot indicates differentiation with respect to cosmic time t, and the appropriate values of n and T are those that pertain at the black hole accretion radius:

$$R_{\rm a} \approx 10^{14} (M/M_\odot) \left(T/10^4\,{\rm K}\right)^{-1} {\rm cm}. \quad 33.$$

Each PBH will initially be surrounded by an HII region of radius $R_{\rm s}$, where the temperature is slightly below 10^4 K and determined by the balance between photoionization heating and inverse Compton cooling from the CMB photons. If $R_{\rm a} > R_{\rm s}$, or if the whole Universe is ionized (so that the individual HII regions have merged), the appropriate values of n and T are those in the background Universe ($\bar{n}$ and $\bar{T}$). In this case, after decoupling, $\dot{M}$ is epoch independent so long as $\bar{T}$ has its usual Friedmann behavior ($\bar{T} \propto z^2$). However, $\dot{M}$ decreases if $\bar{T}$ is boosted above the Friedmann value. If the individual HII regions have not merged and $R_{\rm a} < R_{\rm s}$, the appropriate values for n and T are those within the HII region. In this case, T is close to 10^4 K, and the pressure balance at the edge of the region implies $n \sim \bar{n}\,(\bar{T}/10^4)$ K. Thus, $\dot{M} \propto z^5$ and rapidly decreases until $\bar{T}$ deviates from the standard Friedmann behavior.

If the accreted mass is converted into outgoing radiation with efficiency ϵ, the associated luminosity is

$$L = \epsilon \dot{M} c^2. \quad 34.$$

Annu. Rev. Nucl. Part. Sci. 2020.70:355-394. Downloaded from www.annualreviews.org
Access provided by WIB6263 - Deutsches Elektronen Synchroton (DESY) on 04/08/21. See copyright for approved use.

Reference 12 assumes that both ϵ and the spectrum of emergent radiation are constant. If the spectrum extends up to energy $E_{\max} = 10\eta$ keV, the high-energy photons escape from the individual HII regions unimpeded, so most of the black hole luminosity goes into background radiation or global heating of the Universe through photoionization when the background ionization is low and Compton scattering off electrons when it is high. Reference 12 also assumes that L cannot exceed the Eddington luminosity,

$$L_{\rm ED} = 4\pi\, GM\, m_p/\sigma_T \approx 10^{38}(M/M_\odot)\,{\rm erg\,s^{-1}}, \qquad 35.$$

and it is shown that a PBH will radiate at this limit for some period after decoupling, providing

$$M > M_{\rm ED} \approx 10^3\,\epsilon^{-1}\,\Omega_{\rm g}^{-1}, \qquad 36.$$

where $\Omega_{\rm g}$ is the gas density parameter. The Eddington phase persists until a time $t_{\rm ED}$, which depends on M and $\Omega_{\rm PBH}$ and can be very late for large values of these parameters.

The effect on the thermal history of the Universe is then determined for different $(\Omega_{\rm PBH}, M)$ domains. One has various possible behaviors: In what is termed domain 1, $\bar{T}$ is boosted above 10^4 K, with the Universe being reionized, and possibly up to the temperature of the hottest accretion-generated photons; in domain 2, $\bar{T}$ is boosted to 10^4 K but not above it because of the cooling of the CMB; in domain 3, $\bar{T}$ does not reach 10^4 K, so the Universe is not reionized, but there is a period in which it increases; in domain 4, $\bar{T}$ never increases but follows the CMB temperature, falling like z rather than z^2, for a while; and in domain 5, $\bar{T}$ never deviates from Friedmann behavior.

Constraints on the PBH density in each domain are derived by comparing the time-integrated emission from the PBHs with the observed background intensity in the appropriate waveband (140). For example, in domain 1, the biggest contribution to the background radiation comes from the end of the Eddington phase, and the radiation would currently reside in the range of 0.1 to 1 keV, where $\Omega_{\rm R} \sim 10^{-7}$. The associated limit on the PBH density parameter is then shown to be (140)

$$\Omega_{\rm PBH} < (10\,\epsilon)^{-5/6}\,(M/10^4 M_\odot)^{-5/6}\,\eta^{5/4}\,\Omega_{\rm g}^{-5/6}. \qquad 37.$$

This limit does not apply if the PBH increases its mass appreciably as a result of accretion. During the Eddington phase, each black hole doubles its mass on the Salpeter timescale, $t_{\rm S} \approx 4 \times 10^8\,\epsilon$ years (141), so one expects the mass to increase by a factor $\exp(t_{\rm ED}/t_{\rm S})$ if $t_{\rm ED} > t_{\rm S}$. Because most of the final black hole mass generates radiation with efficiency ϵ, the current energy of the radiation produced is $E(M) \approx \epsilon\, Mc^2/z(M)$, where $z(M)$ is the redshift at which most of the radiation is emitted. This must be less than $z_{\rm S} \approx 10\epsilon^{-2/3}$, the redshift at which the age of the Universe is comparable to $t_{\rm S}$. The current background radiation density is therefore $\Omega_{\rm R} \approx z_{\rm S}^{-1}\epsilon\,\Omega_{\rm PBH}$, so the constraint becomes

$$\Omega_{\rm PBH} < \epsilon^{-1} z_{\rm S}\,\Omega_{\rm R} \approx 10^{-5}\,(10\,\epsilon)^{-5/3}. \qquad 38.$$

This relates to the well-known Sołtan constraint (142) on the growth of the SMBHs that power quasars. The limit given by Equation 37 therefore flattens off at large values of M.

One problem with the above analysis is that the steady-state Bondi formula fails if the accretion timescale,

$$t_B \approx 10^5 (M/10^4 M_\odot)(T/10^4\,{\rm K})^{-3/2}\,{\rm years}, \qquad 39.$$

exceeds the cosmic expansion time, with the solution being described by self-similar infall instead. For $M > 10^4 M_\odot$, this applies at decoupling, and so one has to wait until the time given by Equation 39 for the Bondi formula to apply. Therefore, the above analysis applies only if most of the radiation is generated after this time. Otherwise, the background light limit is weakened.

Annu. Rev. Nucl. Part. Sci. 2020.70:355-394. Downloaded from www.annualreviews.org
Access provided by WIB6263 - Deutsches Elektronen Synchroton (DESY) on 04/08/21. See copyright for approved use.

Later, an improved analysis was provided by Ricotti and colleagues (143). They used a more realistic model for the efficiency parameter ϵ, allowed for the increased density in the dark halo expected to form around each PBH, and included the effect of the velocity dispersion of the PBHs on the accretion in the period after cosmic structures start to form. They found much stronger accretion limits by considering the effects of the emitted radiation on the spectrum and anisotropies of the CMB rather than the background radiation itself. Using FIRAS data to constrain the first, they obtained a limit of $f(M) < (M/1M_\odot)^{-2}$ for $1M_\odot < M \lesssim 10^3 M_\odot$; using WMAP data to constrain the second, they obtained a limit of $f(M) < (M/30M_\odot)^{-2}$ for $30M_\odot < M \lesssim 10^4 M_\odot$. The constraints flatten off above the indicated masses but are taken to extend up to $10^8 M_\odot$. Although these limits appeared to exclude $f = 1$ down to masses as low as $1M_\odot$, they were very model dependent, and there was also a technical error (an incorrect power of redshift) in the calculation.

This problem has been reconsidered by several groups who argue that the limits are weaker than those indicated in Reference 143. Ali-Haïmoud & Kamionkowski (144) calculate the accretion on the assumption that it is suppressed by Compton drag and Compton cooling from CMB photons and allowing for the PBH velocity relative to the background gas. They find that the spectral distortions are too small to be detected, while the anisotropy constraints only exclude $f = 1$ above $10^2 M_\odot$. Their limit is shown by the orange line in **Figure 1**. Horowitz (145) performs a similar analysis and gets an upper limit of $30M_\odot$. Poulin et al. (146) argue that the spherical accretion approximation probably breaks down, with an accretion disk forming instead, which affects the statistical properties of the CMB anisotropies. Provided the disks form early, these constraints exclude a monochromatic distribution of PBH with masses above $2M_\odot$ as the dominant form of dark matter. Because this is the strongest accretion constraint, it is the only one shown in **Figure 1**.

More direct constraints can be obtained by considering the emission of PBHs at the present epoch. For example, Gaggero et al. (147) model the accretion of gas onto a population of massive PBHs in the Milky Way and compare the predicted radio and X-ray emission with observational data. The possibility that $\mathcal{O}(10)M_\odot$ PBHs can provide all of the dark matter is excluded at the 5σ level by a comparison with the VLA radio catalog and the Chandra X-ray catalog. Similar arguments have been made by Manshanden et al. (148). PBH interactions with the interstellar medium should result in a significant X-ray flux that would contribute to the observed number density of compact X-ray objects in galaxies. Inoue & Kusenko (149) use the data to constrain the PBH number density in the mass range from a few to $2 \times 10^7 M_\odot$; their limit is shown in **Figure 1**. However, De Luca et al. (150) have stressed that the change in the mass of PBHs due to accretion may modify the interpretation of the observational bounds on $f(M)$ at the present epoch. In the mass range $10–100M_\odot$, such a change can raise existing upper limits by several orders of magnitude.

3.5. Cosmic Microwave Background Constraints

If PBHs form from the high-σ tail of Gaussian density fluctuations, as in the simplest scenario (48), then another interesting limit comes from the dissipation of these density fluctuations by Silk damping at a much later time. This process leads to a μ distortion in the CMB spectrum (151) for $7 \times 10^6 < t/\mathrm{s} < 3 \times 10^9$, leading to an upper limit of $\delta(M) < \sqrt{\mu} \sim 10^{-2}$ over the mass range $10^3 < M/M_\odot < 10^{12}$. This limit was first given in Reference 62, based on a result in Reference 152, but the limit on μ is now much stronger. There is also a y distortion for $3 \times 10^9 < t/\mathrm{s} < 3 \times 10^{12}$.

This argument gives a very strong constraint on $f(M)$ in the range $10^3 < M/M_\odot < 10^{12}$ (153), but the assumption that the fluctuations are Gaussian may be incorrect. For example, Nakama et al. (154) have proposed a so-called patch model in which the relationship between the background inhomogeneities and the overdensity in the tiny fraction of volumes collapsing to PBHs is

Annu. Rev. Nucl. Part. Sci. 2020.70:355-394. Downloaded from www.annualreviews.org
Access provided by WIB6263 - Deutsches Elektronen Synchroton (DESY) on 04/08/21. See copyright for approved use.

modified, and thus the μ distortion constraint becomes much weaker. Recently, Nakama et al. (155) have used a phenomenological description of non-Gaussianity to calculate the μ distortion constraints on $f(M)$ using the current FIRAS limit and the projected upper limit from PIXIE (156). However, one would need huge non-Gaussianity to avoid the constraints in the mass range of $10^6 M_\odot < M < 10^{10} M_\odot$. Another way out is to assume that the PBHs are initially smaller than the lower limit but undergo substantial accretion between the μ distortion era and the time of matter–radiation equality.

3.6. Gravitational-Wave Constraints

Interest in PBHs has intensified recently because of the detection of GWs from coalescing black hole binaries by LIGO/Virgo (157). Even if these black holes are not of primordial origin, the observations place important constraints on the number of PBHs. Indeed, the LIGO data had already placed weak constraints on such scenarios a decade ago (158). More recent LIGO/Virgo searches find no compact binary systems with component masses in the range of 0.2 to $1.0 M_\odot$ (159). Neither black holes nor neutron stars are expected to form through normal stellar evolution below $1 M_\odot$, and one can infer $f < 0.3$ for $M < 0.2 M_\odot$ and $f < 0.05$ for $M < 1 M_\odot$. A similar search from the second LIGO/Virgo run (160) found constraints on the mergers of $0.2 M_\odot$ and $1.0 M_\odot$ binaries corresponding to at most 16% and 2% of the dark matter, respectively. The possibility that the LIGO/Virgo events relate to PBHs is discussed further in Section 4.4.

A population of massive PBHs would be expected to generate a GW background (GWB) (161), which would be especially interesting if there were a population of binary black holes coalescing at the present epoch because of gravitational-radiation losses. Conversely, the nonobservation of a GWB gives constraints on the fraction of dark matter in PBHs. As shown by Raidal et al. (36), even the early LIGO results gave strong limits in the range $0.5–30 M_\odot$; this limit is shown in **Figure 1**. A similar result was obtained by Wang et al. (162). This constraint has been updated in more recent work using both LIGO/Virgo data (163, 164) and pulsar-timing observations (165). Bartolo et al. (166) calculate the anisotropies and non-Gaussianity of such a stochastic GWB and conclude that PBHs could not provide all the dark matter if these were large.

A different type of GW constraint on $f(M)$ arises because of the large second-order tensor perturbations generated by the scalar perturbations that produce the PBHs (167). The associated frequency was originally given as $10^{-8}\,(M/10^3 M_\odot)$ Hz, but this estimate contained a numerical error (168) and was later reduced by a factor of 10^3 (169). The limit on $f(M)$ just relates to the amplitude of the density fluctuations at the horizon epoch and is of order 10^{-52}. This effect has subsequently been studied by several other authors (170), and limits from LIGO/Virgo and the Big Bang Observer could potentially cover the mass range down to 10^{20} g. Conversely, one can use PBH limits to constrain a background of primordial GWs (171).

The robustness of the LIGO/Virgo bounds on $\mathcal{O}(10) M_\odot$ PBHs depends on the accuracy with which the formation of PBH binaries in the early Universe can be described. Ballesteros et al. (172) revisit the standard estimate of the merger rate and focus on the spatial distribution of nearest neighbors and the expected initial PBH clustering. They confirm the robustness of the previous results in the case of a narrow mass function, which constrains the PBH fraction of dark matter to be $f \sim 0.001–0.01$.

Kühnel et al. (173) investigate GW production by PBHs in the mass range $10^{-13}–1 M_\odot$ orbiting an SMBH. While an individual object would be undetectable, the extended stochastic emission from a large number of such objects might be detectable. In particular, LISA could detect the extended emission from objects orbiting SgrA* at the center of the Milky Way if a dark matter spike, analogous to the WIMP spike predicted by Gondolo & Silk (174), were to form there.

Annu. Rev. Nucl. Part. Sci. 2020.70:355-394. Downloaded from www.annualreviews.org
Access provided by WIB6263 - Deutsches Elektronen Synchroton (DESY) on 04/08/21. See copyright for approved use.

Annu. Rev. Nucl. Part. Sci. 2020.70:355-394. Downloaded from www.annualreviews.org
Access provided by WIB6263 - Deutsches Elektronen Synchroton (DESY) on 04/08/21. See copyright for approved use.

3.7. Interesting Mass Windows and Extended Primordial Black Hole Mass Functions

Figure 1 shows that there are four mass windows (A, B, C, and D) in which PBHs could have an appreciable density, which we somewhat arbitrarily take to mean $f > 0.1$, although the absence of a limit does not mean there is positive evidence for this. The cleanest window would seem to be A, and many of the earlier constraints in this mass range have now been removed. Window C has received the most attention because of the LIGO/Virgo results, but it is challenging to put all the dark matter there because of the large number of constraints in this mass range.

A special comment is required about window D (i.e., the mass range $10^{14} < M/M_\odot < 10^{18}$) because this range has been almost completely neglected in previous literature. Obviously, such stupendously large black holes (which we term SLABs) could not provide the dark matter in galactic halos because they are too large to fit inside them (i.e., they violate the galactic incredulity limit). However, they might provide an intergalactic dark matter component, and the lack of constraints in this mass range may reflect the fact that nobody has considered this possibility. While this proposal might seem exotic, we know there are black holes with masses up to nearly $10^{11} M_\odot$ in galactic nuclei (175), so it is conceivable that SLABs could represent the high-mass tail of such a population. Although PBHs are unlikely to be this large at formation, we have shown in Section 3.4 that they might increase their mass enormously before galaxy formation through accretion, so they could certainly seed SLABs. This possibility has motivated the study of such objects in Reference 176, including an update of the accretion limit mentioned in Section 3.4 and a limit associated with WIMP annihilation, discussed below in Section 6.1. These limits are not shown in **Figure 1**, which is just a summary of previous literature.

The constraints shown in **Figure 1** assume that the PBH mass function is quasi-monochromatic (i.e., width $\Delta M \sim M$). This assumption is unrealistic, and in most scenarios one would expect the mass function to be extended, possibly stretching over several decades of mass. A detailed assessment of this problem requires a knowledge of the expected PBH mass fraction, $f_{\rm exp}(M)$, and the maximum fraction allowed by the monochromatic constraint, $f_{\rm max}(M)$. However, one cannot just plot $f_{\rm exp}(M)$ for a given model in **Figure 1** and infer that the model is allowed because it does not intersect $f_{\rm max}(M)$. This problem is quite challenging, and several different approaches have been suggested.

One approach is to assume that each constraint can be treated as a sequence of flat constraints by breaking it up into narrow mass bins (13), but this is a complicated procedure, and this approach has been criticized by Green (26). A more elegant approach that is similar to Green's was proposed in Reference 27 and also used in Reference 28. In that approach, one introduces the function

$$\psi(M) \propto M \frac{{\rm d}n}{{\rm d}M}, \tag{40.}$$

normalized so that the total fraction of the dark matter in PBHs is

$$f_{\rm PBH} \equiv \frac{\Omega_{\rm PBH}}{\Omega_{\rm CDM}} = \int_{M_{\rm min}}^{M_{\rm max}} {\rm d}M\, \psi(M). \tag{41.}$$

The mass function is specified by the mean and variance of the $\log M$ distribution:

$$\log M_{\rm c} \equiv \langle \log M \rangle_\psi, \quad \sigma^2 \equiv \langle \log^2 M \rangle_\psi - \langle \log M \rangle_\psi^2, \tag{42.}$$

where

$$\langle X \rangle_\psi \equiv f_{\rm PBH}^{-1} \int {\rm d}M\, \psi(M) X(M). \tag{43.}$$

Two parameters should generally suffice locally (i.e., close to a peak) since these just correspond to the first two terms in a Taylor expansion. An astrophysical observable $A[\psi(M)]$ depending on the PBH abundance can generally be expanded as

$$A[\psi(M)] = A_0 + \int \mathrm{d}M\ \psi(M)\, K_1(M) + \int \mathrm{d}M_1\, \mathrm{d}M_2\ \psi(M_1)\, \psi(M_2)\, K_2(M_1, M_2) + \ldots, \qquad 44.$$

where A_0 is the background contribution, and the functions K_j depend on the details of the underlying physics and the nature of the observation. If PBHs with different masses contribute independently to the observable, only the first two terms in Equation 44 need be considered. If a measurement puts an upper bound on the observable,

$$A[\psi(M)] \leq A_{\rm exp}, \qquad 45.$$

then for a monochromatic mass function with $M = M_{\rm c}$ we have

$$\psi_{\rm mon}(M) \equiv f_{\rm PBH}(M_{\rm c})\, \delta(M - M_{\rm c}). \qquad 46.$$

The maximum allowed fraction of dark matter in the PBHs is then

$$f_{\rm PBH}(M_{\rm c}) \leq \frac{A_{\rm exp} - A_0}{K_1(M_{\rm c})} \equiv f_{\rm max}(M_{\rm c}). \qquad 47.$$

Combining Equations 44–47 then yields

$$\int \mathrm{d}M\ \frac{\psi(M)}{f_{\rm max}(M)} \leq 1. \qquad 48.$$

Once $f_{\rm max}$ is known, it is possible to apply Equation 48 for an arbitrary mass function to obtain the constraints equivalent to those for a monochromatic mass function. One first integrates Equation 48 over the mass range (M_1, M_2) for which the constraint applies, assuming a particular function $\psi(M; f_{\rm PBH}, M_{\rm c}, \sigma)$. Once M_1 and M_2 are specified, this constrains $f_{\rm PBH}$ as a function of $M_{\rm c}$ and σ. This procedure must be implemented separately for each observable and each mass function.

In Reference 27, this method is applied for various expected PBH mass functions, while Reference 28 performs a comprehensive analysis for the case in which the PBHs cover the mass range 10^{-18}–$10^{4} M_\odot$. In general, the allowed mass range for fixed $f_{\rm PBH}$ decreases with increasing width σ, thus ruling out the possibility of evading the constraints by simply extending the mass function. However, we stress that the situation could be more complicated than we have assumed above, with more than two parameters being required to describe the PBH mass function. For example, Hasegawa & Kawasaki (177) have proposed an inflationary scenario in the minimally supersymmetric Standard Model that generates both intermediate-mass PBHs to explain the LIGO/Virgo detections and lunar-mass PBHs to explain the dark matter. Section 5 considers a scenario in which the PBH mass function has four peaks, each associated with a particular cosmological conundrum.

4. CLAIMED SIGNATURES

Most of the PBH literature has focused on constraints on their contribution to the dark matter, as reviewed in Section 3. However, a number of papers have claimed positive evidence for them, with masses ranging over 16 orders of magnitude, from $10^{-10} M_\odot$ to $10^{6} M_\odot$. In particular, Reference 54 summarizes seven current observational conundra that may be explained by PBHs. The first three are associated with lensing effects: (*a*) microlensing events toward the Galactic bulge generated by planetary-mass objects (111), which are much more frequent than expected for free-floating planets; (*b*) microlensing of quasars (178), including ones that are so misaligned with the lensing

Annu. Rev. Nucl. Part. Sci. 2020.70:355-394. Downloaded from www.annualreviews.org
Access provided by WIB6263 - Deutsches Elektronen Synchroton (DESY) on 04/08/21. See copyright for approved use.

galaxy that the probability of lensing by a star is very low; and (*c*) the unexpectedly high number of microlensing events toward the Galactic bulge by dark objects in the mass gap between 2 and $5M_\odot$ (179), in which stellar evolution models fail to form black holes (180). The next three are associated with accretion and dynamical effects: (*d*) unexplained correlations in the source-subtracted X-ray and cosmic infrared background fluctuations (181); (*e*) the nonobservation of UFDGs below the critical radius associated with dynamical disruption by PBHs (182); and (*f*) the unexplained correlation between the masses of galaxies and their central SMBHs. The final one is associated with GW effects: (*g*) the observed mass and spin distributions for the coalescing black holes found by LIGO/Virgo. There are additional observational problems that Silk (183) has argued may be solved by PBHs in the intermediate mass range. We now discuss this evidence in more detail, addressing the conundra in order of increasing mass. In Section 5, we discuss how these conundra may have a unified explanation in the scenario proposed in Reference 54.

4.1. Lensing

Observations of M31 by Niikura et al. (106) with the HSC/Subaru telescope have identified a single candidate microlensing event with a mass in the range of $10^{-10} < M < 10^{-6}M_\odot$. Kusenko et al. (184) have argued that nucleation of false vacuum bubbles during inflation could produce PBHs with this mass. Niikura et al. (111) also claim that data from the 5-year OGLE survey of 2,622 microlensing events in the Galactic bulge have revealed six ultrashort events attributable to planetary-mass objects between 10^{-6} and $10^{-4}M_\odot$. These events would contribute about 1% of the CDM—an amount that is much more than expected for free-floating planets (185) and compatible with the bump associated with the electroweak phase transition in the best-fit PBH mass function described in Reference 54.

The MACHO Collaboration originally reported 17 LMC microlensing events and claimed that these were consistent with compact objects of $M \sim 0.5M_\odot$, compatible with PBHs formed at the QCD phase transition (108). Although they concluded that such objects could contribute only 20% of the halo mass, the origin of these events is still a mystery, and this limit is subject to several caveats. Calcino et al. (186) argue that the usual semiisothermal sphere for our halo is no longer consistent with the Milky Way rotation curve. When the uncertainties in the shape of the halo are taken into account, they claim that the LMC microlensing constraints weaken for $M \sim 10M_\odot$ but tighten at lower masses. Hawkins (187) makes a similar point, arguing that low-mass Galactic halo models would relax the constraints and allow 100% of the dark matter to be solar-mass PBHs. Several authors have claimed that PBHs could form in tight clusters—giving a local overdensity well in excess of that provided by the halo concentration alone (84, 188)—and that this increased overdensity may remove the microlensing constraint at $M \sim 1$–$10M_\odot$ altogether, especially if the PBHs have a wide mass distribution.

OGLE has detected around 60 long-duration microlensing events in the Galactic bulge, of which around 20 have GAIA parallax measurements. This breaks the mass-distance degeneracy and implies that these events were probably generated by black holes (179). The event distribution implies a mass function peaking between 0.8 and $5M_\odot$, which overlaps with the gap from 2 to $5M_\odot$ in which black holes are not expected to form as the endpoint of stellar evolution (180). This implication is also consistent with the peak originating from the reduction of pressure at the QCD epoch (54).

Hawkins (189) originally claimed evidence for a critical density of Jupiter-mass PBHs from observations of quasar microlensing. However, his later analysis yielded a lower density (dark matter rather than critical) and a mass of around $1M_\odot$ (190). Mediavilla et al. (178) have also found evidence for quasar microlensing; their findings indicate that 20% of the total mass is in

Annu. Rev. Nucl. Part. Sci. 2020.70:355-394. Downloaded from www.annualreviews.org
Access provided by WIB6263 - Deutsches Elektronen Synchroton (DESY) on 04/08/21. See copyright for approved use.

compact objects in the mass range 0.05–0.45$M_\odot$. These events might be explained by intervening stars, but in several cases the stellar region of the lensing galaxy is not aligned with the quasar; this nonalignment suggests a different population of subsolar halo objects. Hawkins (191) has also argued that some quasar images are best explained as microlensing by PBHs distributed along the lines of sight to the quasars. The best-fit PBH mass function in Reference 54 is consistent with these findings and requires $f_{\rm PBH} \simeq 0.05$ in this mass range.

Recently, Vedantham et al. (192) detected long-term radio variability in the light curves of some active galactic nuclei (AGN). This variability was associated with a pair of strongly skewed peaks in the radio flux density and was observed over a broad frequency range. They propose that this set of circumstances arises from gravitational millilensing of relativistically moving features in the AGN jets, with these features crossing the lensing caustics created by 10^3–$10^6 M_\odot$ subhalo condensates or black holes located within intervening galaxies.

4.2. Dynamical

Lacey & Ostriker (136) once argued that the observed puffing of the Galactic disc could be due to black holes of around $10^6 M_\odot$, with older stars being heated more than younger ones. They claimed that this effect could explain the scaling of the velocity dispersion with age and the relative velocity dispersions in the radial, azimuthal, and vertical directions as well as the existence of a high-velocity tail of stars (193). However, later measurements gave different velocity dispersions for older stars (194), and it is now thought that heating by a combination of spiral density waves and giant molecular clouds may better fit the data (195).

If there were an appreciable number of PBHs in galactic halos, CDM-dominated UFDGs would be dynamically unstable if they were smaller than some critical radius; this radius would also depend on the mass of any central black hole. The nondetection of galaxies smaller than $r_c \sim 10$–20 parsecs, despite their magnitude being above the detection limit, suggests the presence of compact halo objects in the solar-mass range. Moreover, rapid accretion in the densest PBH halos could explain the extreme UFDG mass-to-light ratios observed (182). However, this model may not be supported by a recent analysis by Stegmann et al. (135).

Fuller et al. (196) show that some r-process elements can be produced by the interaction of PBHs with neutron stars if those in the mass range 10^{-14}–$10^{-8} M_\odot$ have $f > 0.01$. When a PBH is captured by a rotating millisecond neutron star, the resulting spin-up ejects $\sim$0.1–0.5$M_\odot$ of relatively cold neutron-rich material. This interaction can also produce a kilonova-type afterglow and a fast radio burst. Abramowicz et al. (197) argue that collisions of neutron stars with PBHs of mass 10^{23} g may explain the millisecond durations and large luminosities of fast radio bursts.

As discussed in Section 3.3, sufficiently large PBHs could generate cosmic structures through the seed or Poisson effect (96); the mass binding at redshift z_B would be

$$\mathcal{M} \approx \begin{cases} 4000\, M\, z_B^{-1} & \text{(seed)} \\ 10^7\, f\, M\, z_B^{-2} & \text{(Poisson)}. \end{cases} \qquad 49.$$

Having $f = 1$ requires $M < 10^3 M_\odot$, and so the Poisson effect could only bind a scale $\mathcal{M} < 10^{10}\, z_B^{-2} M_\odot$, which is necessarily subgalactic. However, this effect would still allow the dwarf galaxies to form earlier than in the standard scenario, which would have interesting observational consequences (183). Having $f \ll 1$ allows the seed effect to be important and raises the possibility that the 10^6–$10^{10} M_\odot$ black holes in AGN are primordial in origin and generate the galaxies. For example, most quasars contain $10^8 M_\odot$ black holes, so it is interesting that this mass suffices to bind a region of mass $10^{11} M_\odot$ at the epoch of galaxy formation. It is sometimes argued that the success of the BBN scenario requires PBHs to form before 1 s, corresponding to a limit of $M < 10^5 M_\odot$.

Annu. Rev. Nucl. Part. Sci. 2020.70:355-394. Downloaded from www.annualreviews.org
Access provided by WIB6263 - Deutsches Elektronen Synchroton (DESY) on 04/08/21. See copyright for approved use.

However, the fraction of the Universe in PBHs at time t is only $10^{-6}\,(t/\mathrm{s})^{1/2}$, so the effect on BBN should be small. Furthermore, the softening of the pressure at e^+e^- annihilation at 10 s naturally produces a peak at $10^6 M_\odot$. As discussed in Section 3.4, such large PBHs would inevitably increase their mass through accretion, so this scenario raises the question of whether a $10^6 M_\odot$ PBH would naturally grow to $10^8 M_\odot$, which would entail a corresponding increase in the value of f.

4.3. X-Ray/Infrared Background

As shown by Kashlinsky and his collaborators (181, 198), the spatial coherence of the X-ray and infrared source-subtracted backgrounds suggests that black holes are required. Although these need not be primordial, the level of the infrared background suggests an overabundance of high-redshift halos, which could be explained by the Poisson effect discussed above if a significant fraction of the CDM comprises solar-mass PBHs. In these halos, a few stars form and emit infrared radiation, while PBHs emit X-rays due to accretion. It is challenging to find other scenarios that naturally produce such features.

4.4. LIGO/Virgo

It has long been appreciated that a key signature of PBHs would be the GWs generated by either their formation (161) (although these would be hard to detect because of redshift effects) or their coalescences if the PBHs formed binaries. Indeed, the detection of coalescing binary black holes was first discussed in Reference 31 in the context of Population III black holes and later in References 33 and 199 in the context of PBHs. However, the precise formation epoch of the black holes is not crucial because the coalescence occurs much later. In either case, the black holes would be expected to cluster inside galactic halos, and so the detection of the GWs would provide a probe of the halo distribution (200).

The suggestion that the dark matter could comprise PBHs has attracted much attention in recent years as a result of the LIGO/Virgo detections (157). To date, 10 events have been observed with component masses in the range 8–$51 M_\odot$. After the first detection, Bird et al. (34) claimed that the expected merger was compatible with the range of 9 to 240 $\mathrm{Gpc}^{-3}\ \mathrm{year}^{-1}$ obtained by the LIGO analysis, and this claim has been supported by other studies (201, 202). However, Sasaki et al. (35) have argued that the lower limit on the merger rate would be in tension with the CMB distortion constraints if the PBHs provided all the dark matter, although one might avoid these constraints if the LIGO/Virgo black holes derived from the accretion and merger of smaller PBHs (201). It should be noted that most of the observed coalesced black holes have effective spins compatible with zero. Although the statistical significance of this result is low (203), it goes against a stellar binary origin (204) but is a prediction of the PBH scenario (205).

If the PBHs have an extended mass function, their density should peak at a lower mass than the coalescence signal. For example, $f^{\mathrm{tot}}_{\mathrm{PBH}} = 1$ but $f_{\mathrm{PBH}}(M) \sim 0.01$ in the range 10–$100 M_\odot$ for the mass distribution covered in Reference 54. Raidal et al. (36) have studied the production and merging of PBH binaries for an extended mass function and possible PBH clustering (cf. Reference 206). They show that PBHs can explain the LIGO/Virgo events without violating any current constraints if they have a log-normal mass function. Subsequent work (163, 164) has studied the formation and disruption of PBH binaries in more detail, using both analytical and numerical calculations for a general mass function. If PBHs make up just 10% of the dark matter, the analytic estimates are reliable and indicate that the constraint from the observed LIGO/Virgo rate is strongest in the mass range 2–$160 M_\odot$, albeit weakened because of the suppression of mergers. Their general conclusion is that the LIGO/Virgo events can result from the mergers of PBHs but that such objects cannot provide all the dark matter unless the PBHs have an extended mass function.

Annu. Rev. Nucl. Part. Sci. 2020.70:355-394. Downloaded from www.annualreviews.org
Access provided by WIB6263 - Deutsches Elektronen Synchroton (DESY) on 04/08/21. See copyright for approved use.

Ali-Haïmoud et al. (37) have computed the probability distribution of orbital parameters for PBH binaries. Their analytic estimates indicate that the tidal field of halos and interactions with other PBHs, as well as dynamical friction by unbound standard dark matter particles, do not provide significant torque on PBH binaries. They also calculate the binary merger rate from gravitational capture in present-day halos. If binaries that formed in the early Universe have survived to the present time, as expected, then they must dominate the total PBH merger rate. Moreover, this merger rate would be above the current LIGO upper limit unless $f(M) < 0.01$ for 10–300$M_\odot$ PBHs.

One of the mass ranges in which PBHs could provide the dark matter is around $10^{-12}M_\odot$. If these PBHs are generated by enhanced scalar perturbations produced during inflation, their formation is inevitably accompanied by the generation of non-Gaussian GWs at frequencies that peak in the mHz range (the maximum sensitivity of LISA). Bartolo et al. (207) have studied whether LISA will be able to detect not only the GW power spectrum but also the non-Gaussian three-point GW correlator (i.e., the bispectrum). However, they conclude that the inclusion of propagation effects suppresses the bispectrum. If PBHs with masses of 10^{20} to 10^{22} g are the dark matter, the corresponding GWs will be detectable by LISA irrespective of the value of $f_{\rm NL}$; this point also has been stressed by Cai et al. (208).

4.5. Arguments for Intermediate-Mass Primordial Black Holes

Silk (183) has argued that intermediate-mass PBHs, which are mostly passive today but were active in their gas-rich past, could be ubiquitous in early dwarf galaxies. This scenario would be allowed by current AGN observations (209), and early feedback from intermediate-mass PBHs could provide a unified explanation for many dwarf galaxy anomalies. Besides providing a phase of early galaxy formation and seeds for SMBHs at high z (discussed above), they could (*a*) suppress the number of luminous dwarfs, (*b*) generate cores in dwarfs by dynamical heating, (*c*) resolve the too-big-to-fail problem, (*d*) create bulgeless disks, (*e*) form UFDGs and ultradiffuse galaxies, (*f*) reduce the baryon fraction in Milky Way–type galaxies, (*g*) explain ultraluminous X-ray sources in the outskirts of galaxies, and (*h*) trigger star formation in dwarfs via AGN. As we discuss in Section 5.1, intermediate-mass PBH production could be naturally triggered by the thermal history of the Universe (54). This would lead to other observational signatures: The intermediate-mass PBHs would generate extreme-mass-ratio inspiral merger events detectable by LISA; they would tidally disrupt white dwarfs much more rapidly than main-sequence stars, leading to luminous flares and short-timescale nuclear transients (210); and they would induce microlensing of extended radio sources (211).

5. UNIFIED PRIMORDIAL BLACK HOLE SCENARIO

In this section, we describe a particular scenario in which PBHs naturally form with an extended mass function and provide a unified explanation of some of the conundra discussed above. The scenario is discussed in detail in Reference 54 and is based on the idea that the thermal history of the Universe leads to dips in the sound-speed and therefore enhanced PBH formation at scales corresponding to the electroweak phase transition ($10^{-6}M_\odot$), the QCD phase transition ($1M_\odot$), the pion plateau ($10M_\odot$), and e^+e^- annihilation ($10^6M_\odot$). This scenario requires most of the dark matter to be in PBHs formed at the QCD peak and is marginally consistent with the constraints discussed in Section 3, even though the discussion in that section suggests that the QCD window cannot provide all the dark matter for a monochromatic PBH mass function.

Annu. Rev. Nucl. Part. Sci. 2020.70:355-394. Downloaded from www.annualreviews.org
Access provided by WIB6263 - Deutsches Elektronen Synchroton (DESY) on 04/08/21. See copyright for approved use.

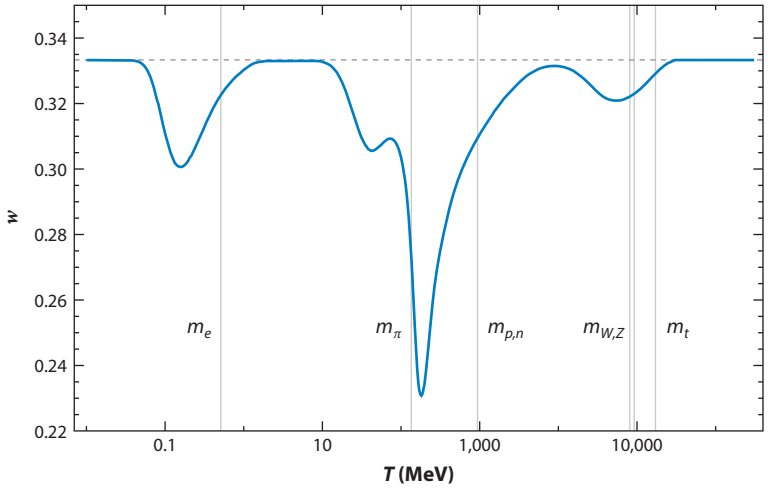

Figure 3

Equation-of-state parameter w as a function of temperature T. The gray vertical lines correspond to the masses of the electron, pion, proton/neutron, W/Z bosons, and top quark, respectively. The gray dashed horizontal lines correspond to $g_* = 100$ and $w = 1/3$. Figure adapted from Reference 54.

5.1. Thermal History of the Universe

Reheating at the end of inflation fills the Universe with radiation. In the Standard Model, the Universe remains dominated by relativistic particles with an energy density that decreases as the fourth power of the temperature. As time increases, the number of relativistic degrees of freedom remains constant until around 200 GeV, at which point the temperature of the Universe falls to the mass thresholds of the Standard Model particles. The first particle to become nonrelativistic is the top quark at 172 GeV, followed by the Higgs boson at 125 GeV, the Z boson at 92 GeV, and the W boson at 81 GeV. At the QCD transition at around 200 MeV, protons, neutrons, and pions condense out of the free light quarks and gluons. A little later, the pions become nonrelativistic and then the muons do, with e^+e^- annihilation and neutrino decoupling occurring at around 1 MeV.

Whenever the number of relativistic degrees of freedom suddenly drops, it changes the effective equation-of-state parameter w. As shown in **Figure 3**, there are four periods in the thermal history of the Universe when w decreases. After each of these, w resumes its relativistic value of $1/3$, but because the threshold δ_c is sensitive to the equation-of-state parameter $w(T)$, the sudden drop modifies the probability of gravitational collapse of any large curvature fluctuations. This results in pronounced features in the PBH mass function even for a uniform power spectrum. If the PBHs form from Gaussian inhomogeneities with root-mean-square amplitude $\delta_{\rm rms}$, then Equation 8 implies that when the temperature of the Universe is T, the fraction of horizon patches undergoing collapse to PBHs is (48)

$$\beta(M) \approx \mathrm{Erfc}\left[\frac{\delta_c\Big(w[T(M)]\Big)}{\sqrt{2}\,\delta_{\rm rms}(M)}\right], \qquad 50.$$

where the value δ_c comes from Reference 40 and the temperature is related to the PBH mass by

$$T \approx 200\sqrt{M_\odot/M}\ \mathrm{MeV}. \qquad 51.$$

Annu. Rev. Nucl. Part. Sci. 2020.70:355-394. Downloaded from www.annualreviews.org
Access provided by WIB6263 - Deutsches Elektronen Synchroton (DESY) on 04/08/21. See copyright for approved use.

Thus, $\beta(M)$ is exponentially sensitive to $w(M)$, and the present CDM fraction for PBHs of mass M is

$$f_{\rm PBH}(M) \equiv \frac{1}{\rho_{\rm CDM}} \frac{{\rm d}\,\rho_{\rm PBH}(M)}{{\rm d}\ln M} \approx 2.4\,\beta(M)\sqrt{\frac{M_{\rm eq}}{M}}, \qquad 52.$$

where $M_{\rm eq} = 2.8 \times 10^{17} M_\odot$ is the horizon mass at matter–radiation equality, and the numerical factor is $2\,(1 + \Omega_B/\Omega_{\rm CDM})$ with $\Omega_{\rm CDM} = 0.245$ and $\Omega_B = 0.0456$ (46). This is equivalent to Equation 7.

There are many inflationary models, and they predict a variety of shapes for $\delta_{\rm rms}(M)$. Some of them produce an extended plateau or dome-like feature in the power spectrum. This effect applies for two-field models like hybrid inflation (22) and even some single-field models like Higgs inflation (212), although this may not apply for the minimal Higgs model (213). Instead of focusing on any specific scenario, Reference 54 assumes a quasi-scale-invariant spectrum:

$$\delta_{\rm rms}(M) = A\left(\frac{M}{M_\odot}\right)^{(1-n_{\rm s})/4}, \qquad 53.$$

where the spectral index $n_{\rm s}$ and amplitude A are treated as free phenomenological parameters. This equation could represent any spectrum with a broad peak, such as might be generically produced by a second phase of slow-roll inflation. The amplitude is chosen to be $A = 0.0661$ for $n_{\rm s} = 0.97$ in order to get an integrated abundance $f^{\rm tot}_{\rm PBH} = 1$. The ratio of the PBH mass to the horizon mass at reentry is denoted by γ, and we assume $\gamma = 0.8$, following References 47 and 214. The resulting mass function is represented in **Figure 4** together with the relevant constraints from Section 3. It exhibits a dominant peak at $M \simeq 2M_\odot$ and three additional bumps at 10^{-5}, 30, and $10^6 M_\odot$.

The discussion in Section 4 has already indicated how these bumps relate to various observational conundra, and further details can be found in Reference 54. Here we emphasize two further

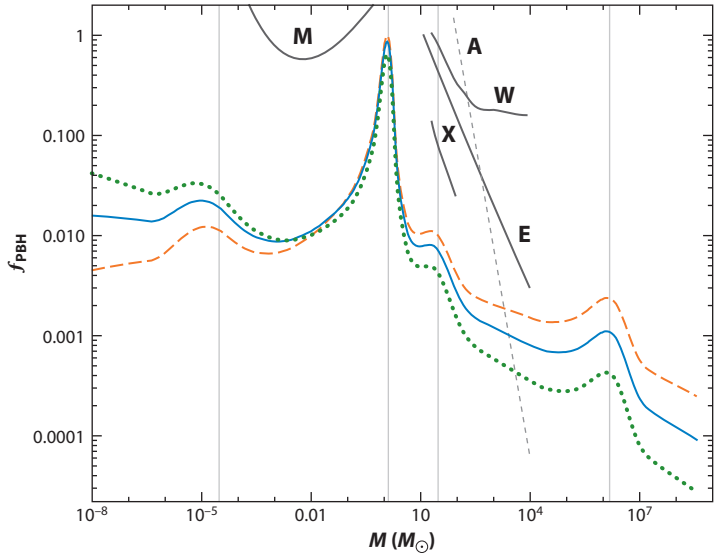

Figure 4

The mass spectrum of primordial black holes (PBHs) with spectral index $n_{\rm s} = 0.965$ (*orange dashed lines*), 0.97 (*blue solid lines*), and 0.975 (*green dotted lines*). The gray vertical lines correspond to the electroweak and QCD phase transitions and e^+e^- annihilation. Also shown are the constraints associated with microlensing (M), wide binaries (W), accretion (A), Eridanus (E), and X-ray observations (X). Figure adapted from Reference 54.

Annu. Rev. Nucl. Part. Sci. 2020.70:355-394. Downloaded from www.annualreviews.org
Access provided by WIB6263 - Deutsches Elektronen Synchroton (DESY) on 04/08/21. See copyright for approved use.

Annu. Rev. Nucl. Part. Sci. 2020.70:355-394. Downloaded from www.annualreviews.org
Access provided by WIB6263 - Deutsches Elektronen Synchroton (DESY) on 04/08/21. See copyright for approved use.

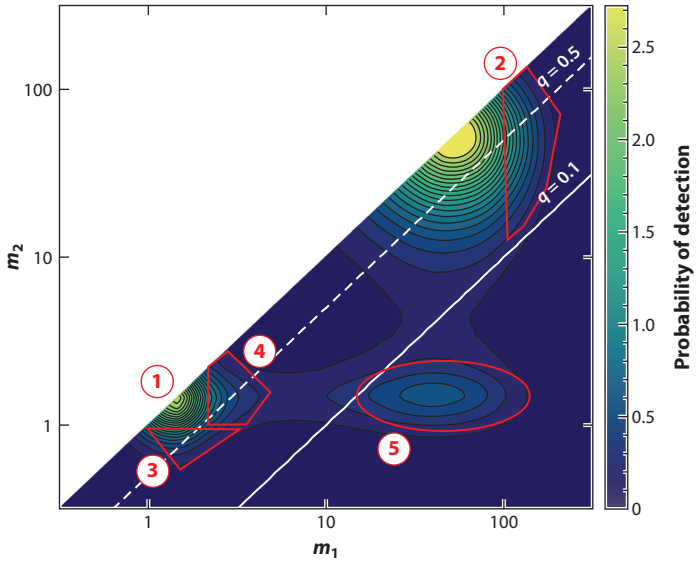

Figure 5

Expected probability distribution of primordial black hole (PBH) mergers with masses m_1 and m_2 (in solar units), assuming a PBH mass function with $n_s = 0.97$ and the LIGO sensitivity for the O2 run. The solid and dashed white lines correspond to mass ratios $q \equiv m_2/m_1$ of 0.1 and 0.5, respectively. The number ① corresponds to the peak for neutron star mergers without electromagnetic counterparts. The mergers of stellar black holes are not expected within the red-bounded regions, which are (②) events with one black hole above $100M_\odot$; (③) mergers of subsolar objects, which might be taken to be neutron stars, with objects at the peak of the black hole distribution; (④) mergers of objects in the mass gap; and (⑤) a subdominant population of mergers with low mass ratios. The color bar indicates the probability of detection. Figure adapted from Reference 54.

features. First, observations of the mass ratios in coalescing binaries provide an important probe of the scenario; the distribution predicted in the unified model is shown in **Figure 5**. The regions outlined by red lines are not occupied by stellar black hole mergers in the standard scenario, and the distinctive prediction is the merger of objects with 1 and $10M_\odot$, corresponding to region 5. Second, for a given PBH mass distribution, one can calculate the number of supermassive PBHs for each halo. There is one $10^8 M_\odot$ PBH per $10^{12} M_\odot$ halo, with 10 times as many smaller ones for $n_s \approx 0.97$ and $f_{\rm PBH}^{\rm tot} \simeq 1$. If one assumes a standard Press-Schechter halo mass function and identifies the PBH mass that has the same number density, one obtains the relation $M_h \approx M_{\rm PBH}/f_{\rm PBH}$, in agreement with observations (215).

5.2. Resolving the Fine-Tuning Problem

The origin of the baryon asymmetry of the Universe (BAU) and the nature of dark matter are two of the most challenging problems in cosmology. The usual assumption is that high-energy physics generates the baryon asymmetry everywhere simultaneously via out-of-equilibrium particle decays or a first-order phase transition at very early times. García-Bellido et al. (214) propose a scenario in which the gravitational collapse of large inhomogeneities at the QCD epoch (invoked above) can resolve both of these problems. The collapse to a PBH is induced by fluctuations of a light spectator scalar field and accompanied by the violent expulsion of surrounding material, which might be regarded as a sort of primordial supernova. This process

provides the ingredients for efficient baryogenesis around the collapsing regions (the baryons subsequently propagate to the rest of the Universe) and naturally explains why the observed BAU is of the order of the PBH collapse fraction (as required by Equation 7) and why the baryons and dark matter have comparable densities.

We now discuss this proposal in more detail. The gravitational collapse of the mass within the QCD Hubble horizon can be extremely violent (40). Particles are driven out as a relativistically expanding shock wave and acquire energies a thousand times their rest mass from the gravitational potential energy released by the collapse. Such high-density hot spots provide the out-of-equilibrium conditions required to generate a baryon asymmetry (216) through the well-known electroweak sphaleron transitions responsible for Higgs windings around the electroweak vacuum (217). In this process, the charge parity (*CP*) symmetry violation of the Standard Model suffices to generate a local baryon-to-photon ratio of order one. The hot spots are separated by many horizon scales, but the outgoing baryons propagate away from the hot spots at the speed of light and become homogeneously distributed well before BBN. The large initial local baryon asymmetry is thus diluted to the tiny observed global BAU.

The energy available for hot spot electroweak baryogenesis can be estimated as follows. Energy conservation implies that the change in kinetic energy due to the collapse of matter within the Hubble radius to the Schwarzschild radius of the PBH is

$$\Delta K \simeq \left(\frac{1}{\gamma} - 1\right) M_{\rm H} = \left(\frac{1-\gamma}{\gamma^2}\right) M_{\rm PBH}. \qquad 54.$$

The energy acquired per proton in the expanding shell is $E_0 = \Delta K/(n_{\rm p}\,\Delta V)$, where $\Delta V = (1-\gamma^3)V_{\rm H}$ is the difference between the Hubble and PBH volumes, so E_0 scales as $(\gamma + \gamma^2 + \gamma^3)^{-1}$. For a PBH formed at $T \approx \Lambda_{\rm QCD} \approx 140$ MeV, the effective temperature is $T_{\rm eff} = 2\,E_0/3 \approx 5$ TeV, which is well above the sphaleron barrier and induces a *CP* violation parameter $\delta_{\rm CP}(T) \sim 10^{-5}(T/20\ {\rm GeV})^{-12}$ (218). The production of baryons can be very efficient, giving $n_{\rm B} \gtrsim n_\gamma$ or $\eta \gtrsim 1$ locally. The scenario is depicted qualitatively in **Figure 6**.

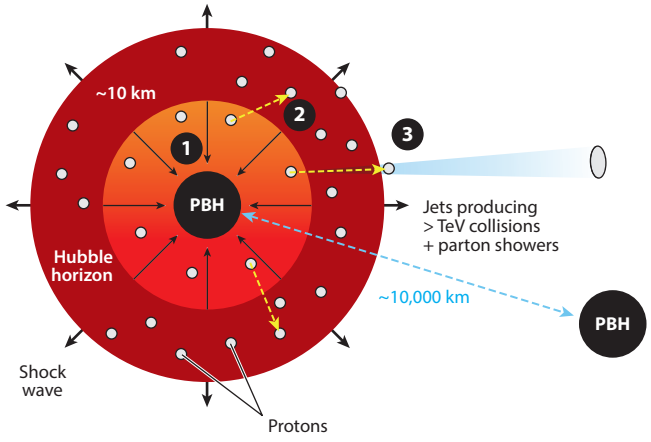

Figure 6

Qualitative representation of the three steps in the discussed scenario. (❶) Gravitational collapse to a primordial black hole (PBH) of the curvature fluctuation at horizon reentry. (❷) Sphaleron transition in hot spot around the PBH, producing $\eta \sim \mathcal{O}(1)$ locally through electroweak baryogenesis. (❸) Propagation of baryons to the rest of the Universe through jets, resulting in the observed baryon asymmetry of the Universe with $\eta \sim 10^{-9}$. Figure adapted from Reference 214.

Annu. Rev. Nucl. Part. Sci. 2020.70:355-394. Downloaded from www.annualreviews.org
Access provided by WIB6263 - Deutsches Elektronen Synchroton (DESY) on 04/08/21. See copyright for approved use.

This proposal naturally links the PBH abundance to the baryon abundance and the BAU to the PBH collapse fraction ($\eta \sim \beta$). The spectator field mechanism for producing the required curvature fluctuations also avoids the need for a fine-tuned peak in the power spectrum, which has long been considered a major drawback of PBH scenarios. One still needs fine-tuning of the mean field value to produce the observed values of η and β (i.e., $\sim 10^{-9}$). However, the stochasticity of the field during inflation ensures that Hubble volumes exist with all possible field values, and thus one can explain the fine-tuning by invoking a single anthropic selection argument. The argument, which is discussed in Reference 47, depends on the fact that only a small fraction of patches will have the PBH and baryon abundance required for galaxies to form. In most patches, the field is too far from the slow-roll region to produce either PBHs or baryons; as a result, radiation universes without any dark matter or matter–antimatter asymmetry are formed. In other (much rarer) patches, PBHs are produced too copiously, leading to rapid accretion of most of the baryons, as might have happened in UFDGs. This anthropic selection effect may therefore explain the observed values of η and β.

6. PRIMORDIAL BLACK HOLE VERSUS PARTICLE DARK MATTER

Presumably, most particle physicists would prefer that the dark matter be made up of elementary particles rather than PBHs, although there is still no direct evidence for this. However, even if the preferred scenario transpires to be the case, PBHs could still play an important cosmological role, so we must distinguish between a scenario in which PBHs provide some dark matter and one in which they provide all of it. This issue also applies for the particle candidates. Nobody would now argue that neutrinos provide the dark matter, but they still play a hugely important role in astrophysics. Therefore, one should not necessarily regard PBHs and particles as rival candidates. Both could exist, and we end this review by discussing two scenarios in this spirit. The first assumes that particles dominate the dark matter but that PBHs still provide an interesting interaction with them. The second involves the notion that evaporating black holes leave stable Planck-mass (or even sub-Planck-mass) relics, although such relics are in some sense more like particles than black holes.

6.1. Combined Primordial Black Hole and Particle Dark Matter

If most of the dark matter is in the form of elementary particles, these will be accreted around any small admixture of PBHs. In the case of WIMPs, this accretion can even happen during the radiation-dominated era; as Eroshenko (219) has shown, a low-velocity subset will accumulate around PBHs as density spikes shortly after the WIMPs kinetically decouple from the background plasma. Their annihilation will give rise to bright γ-ray sources, and comparison of the expected signal with Fermi-LAT data then severely constrains $\Omega_{\rm PBH}$ for $M > 10^{-8} M_\odot$. These constraints are several orders of magnitude more stringent than other constraints if one assumes a WIMP mass of $m_\chi \sim \mathcal{O}(100)$ GeV and the standard value of $\langle \sigma v \rangle_{\rm F} = 3 \times 10^{-26}$ cm s^{-1} for the velocity-averaged annihilation cross-section. Boucenna et al. (220) have investigated this scenario for a larger range of values for $\langle \sigma v \rangle$ and m_χ and reached similar conclusions.

Apart from the early formation of spikes around PBHs that are light enough to arise very early, WIMP accretion around heavier PBHs can also occur by secondary infall (221). This process leads to a different halo profile, which yields a constraint of $f_{\rm PBH} \lesssim \mathcal{O}(10^{-9})$ for the same values of $\langle \sigma v \rangle$ and m_χ. While Adamek et al. (222) have derived this limit for solar-mass PBHs, the argument can be extended to much bigger masses, even up to the values associated with SLABs (176). The constraint at intermediate M comes from the integrated effect of a population of such objects and

Annu. Rev. Nucl. Part. Sci. 2020.70:355-394. Downloaded from www.annualreviews.org
Access provided by WIB6263 - Deutsches Elektronen Synchroton (DESY) on 04/08/21. See copyright for approved use.

is flat:

$$f_{\rm PBH} < \frac{16}{3}\frac{\Phi^{\rm Fermi}_{100\,\rm MeV}\,H_0}{\rho_{\rm DM}\,\tilde{N}_\gamma(m_\chi)}\left(\frac{2\,m_\chi^4\,t_0^2}{\langle\sigma\,v\rangle\,\rho_{\rm eq}}\right)^{1/3}, \qquad 55.$$

where $\Phi^{\rm Fermi}_{100\,\rm MeV} = 6 \times 10^{-9}$ cm^{-2} s^{-1} is the Fermi point-source sensitivity above the threshold energy $E_{\rm th} = 100$ MeV, t_0 is the age of the Universe, and $\rho_{\rm eq} = 2.1 \times 10^{-19}$ g cm^{-3} is the density at $t_{\rm eq}$. $\tilde{N}_\gamma$ is the average number of photons produced,

$$\tilde{N}_\gamma(m_\chi) \equiv \int_{E_{\rm th}}^{m_\chi} {\rm d}E\,\frac{{\rm d}N_\gamma}{{\rm d}E}\int_0^\infty {\rm d}z\,\frac{H_0}{H(z)}\,e^{-\tau_E(z,\,E)}, \qquad 56.$$

where ${\rm d}N_\gamma/{\rm d}E$ is the number of γ-rays emitted from the annihilations occurring per unit of time and energy. The optical depth τ_E is the result of processes such as photon–matter pair production, photon–photon scattering, and photon–photon pair production (223). The limit shown by Equation 55 is derived in Reference 176 using the numerical packages from Reference 224 to obtain the optical depth and spectrum of by-products from WIMP annihilations.

Figure 7 shows constraints on $f_{\rm PBH}$ for WIMP masses of 10 GeV, 100 GeV, and 1 TeV. The falling part at low M is associated with halos formed after dark matter kinetic decoupling (when the kinetic energy of the WIMPs is important); the flat part is associated with halos formed by secondary infall at later times (when the kinetic energy can be neglected). No bound can be placed above the masses at which the lines intersect the incredulity limit:

$$M_{\rm IL} = 2.5 \times 10^{10} M_\odot \left(\frac{m_\chi}{100\,\rm GeV}\right)^{1.11}\left(\frac{\langle\sigma\,v\rangle}{\langle\sigma\,v\rangle_{\rm F}}\right)^{-1/3}. \qquad 57.$$

For axion-like particles or sterile neutrinos, there is a similar limit but from decays rather than annihilations. Kühnel & Ohlsson (225) have derived bounds on the axion-like particle and found

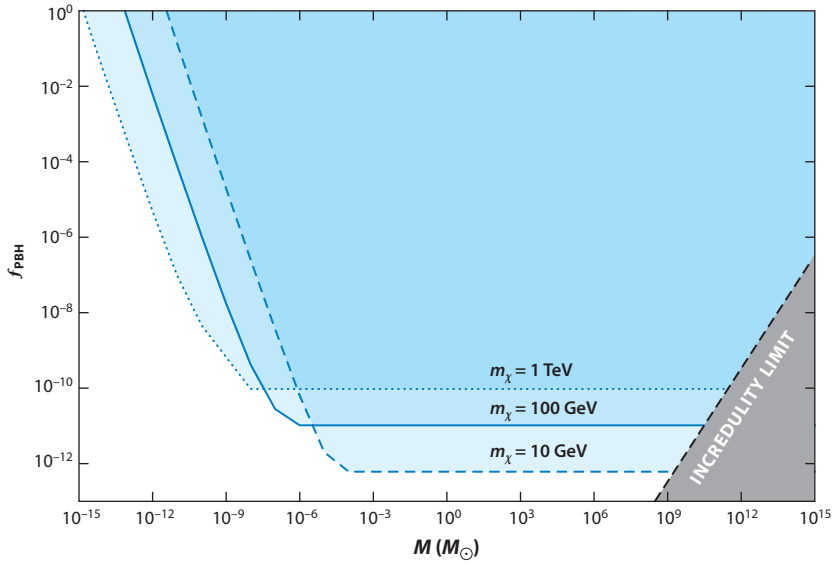

Figure 7

Constraints on $f_{\rm PBH}$ as a function of primordial black hole (PBH) mass for weakly interacting massive particle masses of 10 GeV (*blue dashed line*), 100 GeV (*blue solid line*), and 1 TeV (*blue dotted line*), with $\langle\sigma\,v\rangle = 3 \times 10^{-26}$ cm^3 s^{-1}. Also shown is the incredulity limit (*black dashed line*), which corresponds to one PBH per horizon. Figure adapted from Reference 176.

Annu. Rev. Nucl. Part. Sci. 2020.70:355-394. Downloaded from www.annualreviews.org
Access provided by WIB6263 - Deutsches Elektronen Synchroton (DESY) on 04/08/21. See copyright for approved use.

that the detection prospects for axion-like particle masses below $\mathcal{O}(1)$ keV and halos heavier than $10^{-5} M_\odot$ are far better than for the pure axion-like particle scenario. For sterile-neutrino halos, there are good detection prospects for X-ray, γ-ray, and neutrino telescopes (226, 227).

6.2. Planck-Mass Relics

If PBH evaporations leave stable Planck-mass relics, these might also contribute to the dark matter. This was first pointed out by MacGibbon (228) and subsequently explored in the context of inflationary scenarios by several other authors (58, 229). If the relics have a mass $\kappa\, M_{\rm Pl}$ and reheating occurs at a temperature $T_{\rm R}$, then the requirement that they have less than the critical density implies (58)

$$\beta'(M) < 2 \times 10^{-28}\, \kappa^{-1} \left(\frac{M}{M_{\rm Pl}}\right)^{3/2} \qquad 58.$$

for the mass range

$$\left(\frac{T_{\rm Pl}}{T_{\rm R}}\right)^2 < \frac{M}{M_{\rm Pl}} < 10^{11}\, \kappa^{2/5}. \qquad 59.$$

One would then require the density to be less than $\Omega_{\rm CDM} \approx 0.26$, which strengthens the original limit by a factor of four. The lower mass limit arises because PBHs generated before reheating are diluted exponentially. The upper mass limit arises because PBHs larger than this dominate the total density before they evaporate, in which case the final cosmological baryon-to-photon ratio is determined by the baryon asymmetry associated with their emission. The limit from Equation 58 still applies even if there is no inflationary period, but in that case it extends all the way down to the Planck mass.

It is usually assumed that such relics would be undetectable apart from their gravitational effects. However, Lehmann et al. (230) have recently pointed out that these relics may carry electric charge, which would make them visible to terrestrial detectors. Lehmann et al. evaluate constraints and detection prospects and show that this scenario, if not already ruled out by monopole searches, can be explored within the next decade with planned experiments.

In some scenarios, PBHs could leave stable relics whose masses are very different from the Planck mass. For example, if one maintains the Schwarzschild expression but adopts the Generalized Uncertainty Principle, in which $\Delta x \sim 1/\Delta p + \alpha\, \Delta p$, then evaporation stops at a mass of $\sqrt{\alpha}\, M_{\rm Pl}$ (231). However, if one adopts the Black Hole Uncertainty Principle correspondence (232), in which one has a unified expression for the Schwarzschild and Compton scales, $R_{\rm CS} = 2\, GM + \beta\, M_{\rm Pl}^2/M$, then the mass can fall into the sub-Planckian regime in which $T \propto M$. In this case, evaporation stops when the black hole becomes cooler than the CMB at $M \sim 10^{-36}$ g (233). One motivation for this correspondence is Dvali & Gomez's framework (234) for black holes as graviton Bose-Einstein condensates. Kühnel & Sandstad (235) have studied PBH formation in this context and argue that evaporation may stop because the gravitons are quantum-depleted much faster than the baryons or leptons, which are caught in the black hole condensate. So, at some point, the balance of the strong and gravitational forces leads to stable relics. Recently, Dvali et al. (236) have shown that the decay of a black hole is substantially suppressed because of its high capacity for memory storage, which also leads to extremely long-lived or even stable relics.

7. CONCLUSIONS

While the study of PBHs has been a niche interest for most of the last 50 years, they have become the focus of increasing attention recently. This is strikingly reflected in the publication rate on the topic, which has now risen to several hundred publications per year. While the evidence for PBHs

Annu. Rev. Nucl. Part. Sci. 2020.70:355-394. Downloaded from www.annualreviews.org
Access provided by WIB6263 - Deutsches Elektronen Synchroton (DESY) on 04/08/21. See copyright for approved use.

is far from conclusive, there is a growing appreciation of their many potential roles in cosmology and astrophysics, which is why we have stressed the possible evidence for PBHs in this review rather than just the constraints.

PBHs have been invoked for three main purposes: (*a*) to explain the dark matter, (*b*) to generate the observed LIGO/Virgo coalescences, and (*c*) to provide seeds for the SMBHs in galactic nuclei. The discussion in Section 5 suggests that they could explain several other observational conundra and also alleviate some of the well-known problems of the CDM scenario. Thus, PBHs could play an important cosmological role even if most of the dark matter transpires to be elementary particles.

Regarding the first of these main purposes, there are only a few mass ranges in which PBHs could provide the dark matter. We have focused on the intermediate mass range of $10M_\odot < M < 10^2 M_\odot$ because this may be relevant to the second main purpose, but the sublunar range 10^{20}–10^{24} g and the asteroid range 10^{16}–10^{17} g have also been suggested. If the PBHs have a monochromatic mass function, the discussion in Section 3 suggests that only the lowest mass range is viable. However, the discussion in Section 5 indicates that this conclusion may not apply if the PBHs have an extended mass function.

Regarding the second main purpose, while the possibility that the LIGO/Virgo sources could be PBHs is acknowledged by the GW community, this is not the mainstream view. It is therefore important to stress that the next LIGO/Virgo runs should be able to test and possibly eliminate the PBH proposal. Indeed, the two recent events GW190425 and GW190814 (237) fall precisely within regions 4 and 5 of **Figure 5**, while a third event, GW190521 (238), falls within region 2. In any case, this scenario would not require the PBHs to provide all the dark matter. If the PBHs have an extended mass function, the mass at which the density peaks would be less than the mass that dominates the GW signal.

Regarding the third main purpose, there is no reason in principle why the maximum mass of a PBH should not be in the supermassive range, in which case it is almost inevitable that PBHs could seed SMBHs and perhaps even galaxies themselves. The main issue is whether there are enough PBHs to do so, but this would only require them to have a very low cosmological density. While the mainstream assumption is that galaxies form first, with the SMBHs forming in their nuclei through dynamical processes, this scenario is not fully understood. A crucial question concerns the growth of such large black holes, and this question applies whether or not they are primordial.

Section 5 has described a scenario in which PBHs form with a bumpy mass function as a result of naturally occurring dips in the sound-speed at various cosmological epochs, this naturally explaining many cosmological conundra. This scenario also suggests that the cosmological baryon asymmetry may be generated by PBH formation at the QCD epoch, thus naturally explaining the fine-tuning in the collapse fraction. This is not the mainstream view for the origin of the baryon asymmetry, and the proposal requires further investigation, but this is a first attempt to address the much-neglected PBH fine-tuning problem. The possibility that evaporating PBHs might leave stable relics opens up some of the mass range below 10^{15} g as a new world of compact dark matter candidates waiting to be explored.

DISCLOSURE STATEMENT

The authors are not aware of any affiliations, memberships, funding, or financial holdings that might be perceived as affecting the objectivity of this review.

ACKNOWLEDGMENTS

We are grateful to Sebastien Clesse, Juan García-Bellido, Kazunori Kohri, Marit Sandstad, Yuuiti Sendouda, Luca Visinelli, and Jun-ichi Yokoyama, some of our joint work with whom is reported in

Annu. Rev. Nucl. Part. Sci. 2020.70:355-394. Downloaded from www.annualreviews.org
Access provided by WIB6263 - Deutsches Elektronen Synchroton (DESY) on 04/08/21. See copyright for approved use.

this review. We also thank our many other PBH collaborators and apologize that not all of their important papers are cited because of the limit on the number of references. Helpful remarks from Yacine Ali-Haïmoud, Chris Belczynski, Valerio de Luca, Sasha Dolgov, Xiao Fang, Gabriele Francolini, Cristiano Germani, Anne Green, Qing-Guo Huang, Ranjan Laha, Paulo Monteiro-Camacho, Shi Pi, Martti Raidal, Javier Rubio, Toni Riotto, Jakob Stegmann, Haijun Tian, Matteo Viel, Sai Wang, and Miguel Zumalacárregui are warmly acknowledged. B.C. thanks the Research Center for the Early Universe (RESCEU) of the University of Tokyo, and F.K. thanks the Oskar Klein Centre for Cosmoparticle Physics, Queen Mary University of London, and the Delta Institute for Theoretical Physics for hospitality and support. F.K. also acknowledges support from the Swedish Research Council through contract 638-2013-8993.

Annu. Rev. Nucl. Part. Sci. 2020.70:355-394. Downloaded from www.annualreviews.org
Access provided by WIB6263 - Deutsches Elektronen Synchroton (DESY) on 04/08/21. See copyright for approved use.

LITERATURE CITED

1. Zel'dovich YB, Novikov I. *Sov. Astron.* 10:602 (1967)
2. Hawking SW. *Nature* 248:30 (1974)
3. Carr BJ, Kohri K, Sendouda Y, Yokoyama J. *Phys. Rev. D* 81:104019 (2010)
4. Page DN, Hawking SW. *Astrophys. J.* 206:1 (1976); Carr BJ. *Astrophys. J.* 206:8 (1976)
5. Wright EL. *Astrophys. J.* 459:487 (1996); Lehoucq R, Casse M, Casandjian JM, Grenier I. *Astron. Astrophys.* 502:37 (2009)
6. Kiraly P, Szabelski J, Wdowczyk J, Wolfendale AW. *Nature* 293:120 (1981); MacGibbon JH, Carr BJ. *Astrophys. J.* 371:447 (1991)
7. Okele PN, Rees MJ. *Astron. Astrophys.* 81:263 (1980); Bambi C, Dolgov AD, Petrov AA. *Phys. Lett. B* 670:174 (2008). Erratum. *Phys. Lett. B* 681:504 (2009)
8. Belotsky KM, Kirillov AA. *J. Cosmol. Astropart. Phys.* 1501:041 (2015)
9. Belyanin AA, Kocharovsky VV, Kocharovsky VV. *Mon. Not. R. Astron. Soc.* 283:626 (1996); Cline DB, Sanders DA, Hong W. *Astrophys. J.* 486:169 (1997)
10. Carr BJ, Rees MJ. *Mon. Not. R. Astron. Soc.* 206:801 (1984); Bean R, Magueijo J. *Phys. Rev. D* 66:063505 (2002)
11. Mészáros P. *Astron. Astrophys.* 38:5 (1975)
12. Carr BJ. *Mon. Not. R. Astron. Soc.* 194:639 (1981)
13. Carr B, Kühnel F, Sandstad M. *Phys. Rev. D* 94:083504 (2016)
14. Chapline GF. *Nature* 253:251 (1975)
15. Cyburt RH, Fields BD, Olive KA. *Phys. Lett. B* 567:227 (2003)
16. Frampton PH. *Mod. Phys. Lett. A* 31:1650093 (2016)
17. Alcock C, et al. *Astrophys. J.* 486:697 (1997)
18. Jedamzik K. *Phys. Rep.* 307:155 (1998)
19. Alcock C, et al. *Astrophys. J.* 542:281 (2000); Tisserand P, et al. *Astron. Astrophys.* 469:387 (2007)
20. Carr B, Kohri K, Sendouda Y, Yokoyama J. arXiv:2002.12778 [astro-ph.CO] (2020)
21. Inomata K, et al. *Phys. Rev. D* 96:043504 (2017)
22. Clesse S, García-Bellido J. *Phys. Rev. D* 92:023524 (2015)
23. Byrnes CT, Hindmarsh M, Young S, Hawkins MRS. *J. Cosmol. Astropart. Phys.* 1808:041 (2018)
24. Dolgov A, Silk J. *Phys. Rev. D* 47:4244 (1993)
25. Yokoyama J. *Phys. Rev. D* 58:107502 (1998)
26. Green AM. *Phys. Rev. D* 94:063530 (2016)
27. Carr B, et al. *Phys. Rev. D* 96:023514 (2017)
28. Kühnel F, Freese K. *Phys. Rev. D* 95:083508 (2017)
29. Abbott BP, et al. *Phys. Rev. X* 6:041015 (2016). Erratum. *Phys. Rev. X* 8:039903 (2018); Abbott B, et al. *Phys. Rev. Lett.* 116:241102 (2016); Abbott BP, et al. *Astrophys. J. Lett.* 882:L24 (2019)
30. Belczynski K, Holz DE, Bulik T, O'Shaughnessy R. *Nature* 534:512 (2016)
31. Bond JR, Carr BJ. *Mon. Not. R. Astron. Soc.* 207:585 (1984)
32. Kinugawa T, et al. *Mon. Not. R. Astron. Soc.* 442:2963 (2014)

Annu. Rev. Nucl. Part. Sci. 2020.70:355-394. Downloaded from www.annualreviews.org
Access provided by WIB6263 - Deutsches Elektronen Synchroton (DESY) on 04/08/21. See copyright for approved use.

33. Nakamura T, Sasaki M, Tanaka T, Thorne KS. *Astrophys. J. Lett.* 487:L139 (1997)
34. Bird S, et al. *Phys. Rev. Lett.* 116:201301 (2016)
35. Sasaki M, Suyama T, Tanaka T, Yokoyama S. *Phys. Rev. Lett.* 117:061101 (2016). Erratum. *Phys. Rev. Lett.* 121:059901 (2018); Nakamura T, et al. *Prog. Theor. Exp. Phys.* 2016:093E01 (2016); Sasaki M, Suyama T, Tanaka T, Yokoyama S. *Class. Quant. Grav.* 35:063001 (2018)
36. Raidal M, Vaskonen V, Veerme H. *J. Cosmol. Astropart. Phys.* 1709:037 (2017)
37. Ali-Haïmoud Y, Kovetz ED, Kamionkowski M. *Phys. Rev. D* 96:123523 (2017)
38. Hawking S. *Mon. Not. R. Astron. Soc.* 152:75 (1971); Carr BJ, Hawking SW. *Mon. Not. R. Astron. Soc.* 168:399 (1974)
39. Gundlach C. *Living Rev. Rel.* 2:4 (1999)
40. Musco I, Miller JC. *Class. Quant. Grav.* 30:145009 (2013)
41. Gundlach C. *Phys. Rep.* 376:339 (2003)
42. Niemeyer JC, Jedamzik K. *Phys. Rev. Lett.* 80:5481 (1998); Niemeyer JC, Jedamzik K. *Phys. Rev. D* 59:124013 (1999); Shibata M, Sasaki M. *Phys. Rev. D* 60:084002 (1999); Musco I, Miller JC, Rezzolla L. *Class. Quant. Grav.* 22:1405 (2005); Musco I, Miller JC, Polnarev AG. *Class. Quant. Grav.* 26:235001 (2009)
43. Kühnel F, Rampf C, Sandstad M. *Eur. Phys. J. C* 76:93 (2016)
44. Ade PAR, et al. *Astron. Astrophys.* 594:A20 (2016)
45. Hinshaw G, et al. *Astrophys. J. Suppl.* 180:225 (2009)
46. Aghanim N, et al. arXiv:1807.06209 [astro-ph.CO] (2018)
47. Carr B, Clesse S, García-Bellido J. arXiv:1904.02129 [astro-ph.CO] (2019)
48. Carr BJ. *Astrophys. J.* 201:1 (1975)
49. Harada T, Yoo CM, Kohri K. *Phys. Rev. D* 88:084051 (2013). Erratum. *Phys. Rev. D* 89:029903 (2014)
50. Musco I. *Phys. Rev. D* 100:123524 (2019); Germani C, Sheth RK. *Phys. Rev. D* 101:063520 (2020)
51. Escriva A, Germani C, Sheth RK. *Phys. Rev. D* 101:044022 (2020); Escriva A, Germani C, Sheth RK. arXiv:2007.05564 [gr-qc] (2020)
52. Atal V, Germani C. *Phys. Dark Univ.* 24:100275 (2019); Kehagias A, Musco I, Riotto A. *J. Cosmol. Astropart. Phys.* 1912:029 (2019)
53. Kühnel F, Sandstad M. *Phys. Rev. D* 94:063514 (2016); Germani C, Musco I. *Phys. Rev. Lett.* 122:141302 (2019); Escriva A. *Phys. Dark Univ.* 27:100466 (2020)
54. Carr B, Clesse S, García-Bellido J, Kühnel F. arXiv:1906.08217 [astro-ph.CO] (2019)
55. Harrison ER. *Phys. Rev. D* 1:2726 (1970); Zeldovich YB. *Mon. Not. R. Astron. Soc.* 160:1P (1972)
56. Khlopov MY, Polnarev AG. *Phys. Lett. B* 97:383 (1980); Polnarev AG, Khlopov MY. *Sov. Astron.* 26:391 (1982)
57. Khlopov MY, Malomed BA, Zeldovich YB. *Mon. Not. R. Astron. Soc.* 215:575 (1985)
58. Carr BJ, Gilbert JH, Lidsey JE. *Phys. Rev. D* 50:4853 (1994)
59. Hidalgo JC, et al. *Phys. Rev. D* 96:063504 (2017)
60. Harada T, et al. *Astrophys. J.* 833:61 (2016)
61. Carr B, Tenkanen T, Vaskonen V. *Phys. Rev. D* 96:063507 (2017)
62. Carr BJ, Lidsey JE. *Phys. Rev. D* 48:543 (1993); Ivanov P, Naselsky P, Novikov I. *Phys. Rev. D* 50:7173 (1994); García-Bellido J, Linde AD, Wands D. *Phys. Rev. D* 54:6040 (1996); Randall L, Soljacic M, Guth AH. *Nucl. Phys. B* 472:377 (1996)
63. Dolgov A, Kawasaki M, Kevlishvili N. *Nucl. Phys. B* 807:229 (2009)
64. Kannike K, Marzola L, Raidal M, Veermae H. *J. Cosmol. Astropart. Phys.* 1709:020 (2017)
65. Inomata K, et al. *Phys. Rev. D* 95:123510 (2017)
66. Vilenkin A. *Phys. Rev. D* 27:2848 (1983); Starobinsky AA. *Lect. Notes Phys.* 246:107 (1986); Linde AD. *Phys. Lett. B* 175:395 (1986)
67. Pattison C, Vennin V, Assadullahi H, Wands D. *J. Cosmol. Astropart. Phys.* 1710:046 (2017)
68. Kühnel F, Freese K. *Eur. Phys. J. C* 79:954 (2019)
69. Kühnel F, Schwarz DJ. *Phys. Rev. D* 78:103501 (2008); Kühnel F, Schwarz DJ. *Phys. Rev. D* 79:044009 (2009); Kühnel F, Schwarz DJ. *Phys. Rev. Lett.* 105:211302 (2010)
70. Ezquiaga JM, García-Bellido J. *J. Cosmol. Astropart. Phys.* 1808:018 (2018); Ezquiaga JM, García-Bellido J, Vennin V. *J. Cosmol. Astropart. Phys.* 2003:029 (2020)

Annu. Rev. Nucl. Part. Sci. 2020.70:355-394. Downloaded from www.annualreviews.org
Access provided by WIB6263 - Deutsches Elektronen Synchroton (DESY) on 04/08/21. See copyright for approved use.

71. Choptuik MW. *Phys. Rev. Lett.* 70:9 (1993)
72. Koike T, Hara T, Adachi S. *Phys. Rev. Lett.* 74:5170 (1995)
73. Evans CR, Coleman JS. *Phys. Rev. Lett.* 72:1782 (1994)
74. Yokoyama J. *Phys. Rep.* 307:133 (1998)
75. Crawford M, Schramm DN. *Nature* 298:538 (1982)
76. Jedamzik K. *Phys. Rev. D* 55:R5871 (1997)
77. Schmid C, Schwarz DJ, Widerin P. *Phys. Rev. D* 59:043517 (1999); Widerin P, Schmid C. arXiv:astro-ph/9808142 (1998)
78. Caldwell RR, Casper P. arXiv:gr-qc/9509012 [gr-qc] (1995)
79. Hawking S. *Phys. Lett. B* 231:237 (1989)
80. Polnarev A, Zembowicz R. *Phys. Rev. D* 43:1106 (1991); Garriga J, Sakellariadou M. *Phys. Rev. D* 48:2502 (1993); Caldwell RR, Casper P. *Phys. Rev. D* 53:3002 (1996); MacGibbon JH, Brandenberger RH, Wichoski UF. *Phys. Rev. D* 57:2158 (1998); Jenkins AC, Sakellariadou M. arXiv:2006.16249 [astro-ph.CO] (2020)
81. Hawking SW, Moss IG, Stewart JM. *Phys. Rev. D* 26:2681 (1982); Kodama H, Sasaki M, Sato K. *Prog. Theor. Phys.* 68:1979 (1982); Leach SM, Grivell IJ, Liddle AR. *Phys. Rev. D* 62:043516 (2000); Moss IG. *Phys. Rev. D* 50:676 (1994); Kitajima N, Takahashi F. arXiv: 2006.13137 [hep-ph] (2020)
82. Kodama H, Sasaki M, Sato K, Maeda K. *Prog. Theor. Phys.* 66:2052 (1981); Maeda K. *Class. Quant. Grav.* 3:233 (1986)
83. Khlopov MY, Konoplich RV, Rubin SG, Sakharov AS. arXiv:hep-ph/9807343 [hep-ph] (1998); Konoplich RV, Rubin SG, Sakharov AS, Khlopov MY. *Phys. At. Nucl.* 62:1593 (1999) [*Yad. Fiz.* 62:1705 (1999)]; Khlopov MY, Konoplich RV, Rubin SG, Sakharov AS. *Grav. Cosmol.* 2:S1 (1999); Khlopov MY, Konoplich RV, Rubin SG, Sakharov AS. *Grav. Cosmol.* 6:153 (2000)
84. Dokuchaev V, Eroshenko Y, Rubin S. *Grav. Cosmol.* 11:99 (2005)
85. Rubin SG, Sakharov AS, Khlopov MY. *J. Exp. Theor. Phys.* 91:921 (2001) [*J. Exp. Theor. Phys.* 92:921 (2001)]
86. Garriga J, Vilenkin A, Zhang J. *J. Cosmol. Astropart. Phys.* 1602:064 (2016); Deng H, Garriga J, Vilenkin A. *J. Cosmol. Astropart. Phys.* 1704:050 (2017)
87. Deng H, Vilenkin A. *J. Cosmol. Astropart. Phys.* 1712:044 (2017); Liu J, Guo ZK, Cai RG. *Phys. Rev. D* 101:023513 (2020)
88. Young S, Byrnes CT. *J. Cosmol. Astropart. Phys.* 1308:052 (2013); Bugaev EV, Klimai PA. *Int. J. Mod. Phys. D* 22:1350034 (2013)
89. Bugaev E, Klimai P. *Phys. Rev. D* 85:103504 (2012); Bugaev E, Klimai P. *J. Cosmol. Astropart. Phys.* 1111:028 (2011); Sasaki M, Valiviita J, Wands D. *Phys. Rev. D* 74:103003 (2006)
90. Young S, Byrnes CT. *J. Cosmol. Astropart. Phys.* 1504:034 (2015); Tada Y, Yokoyama S. *Phys. Rev. D* 91:123534 (2015)
91. Linde AD. *Phys. Rev. D* 49:748 (1994)
92. Sheth RK, Mo HJ, Tormen G. *Mon. Not. R. Astron. Soc.* 323:1 (2001)
93. Cai YF, Tong X, Wang DG, Yan SF. *Phys. Rev. Lett.* 121:081306 (2018)
94. Carr B, Kühnel F. *Phys. Rev. D* 99:103535 (2019)
95. García-Bellido J. *Proc. Sci.* EDSU2018:042 (2018)
96. Carr B, Silk J. *Mon. Not. R. Astron. Soc.* 478:3756 (2018)
97. Carr BJ, Kohri K, Sendouda Y, Yokoyama J. *Phys. Rev. D* 94:044029 (2016)
98. Boudaud M, Cirelli M. *Phys. Rev. Lett.* 122:041104 (2019)
99. Laha R. *Phys. Rev. Lett.* 123:251101 (2019)
100. DeRocco W, Graham PW. *Phys. Rev. Lett.* 123:251102 (2019)
101. Laha R, Muñoz JB, Slatyer TR. *Phys. Rev. D* 101:123514 (2020); Chan MH, Lee CM. arXiv:2007.05677 [astro-ph.HE] (2020)
102. Marani GF, et al. *Astrophys. J. Lett.* 512:L13 (1999); Nemiroff RJ, Marani GF, Norris JP, Bonnell JT. *Phys. Rev. Lett.* 86:580 (2001)
103. Barnacka A, Glicenstein JF, Moderski R. *Phys. Rev. D* 86:043001 (2012)
104. Katz A, Kopp J, Sibiryakov S, Xue W. *J. Cosmol. Astropart. Phys.* 1812:005 (2018)

105. Griest K, Cieplak AM, Lehner MJ. *Phys. Rev. Lett.* 111:181302 (2013); Griest K, Cieplak AM, Lehner MJ. *Astrophys. J.* 786:158 (2014)
106. Niikura H, et al. *Nat. Astron.* 3:524 (2019)
107. Paczynski B. *Astrophys. J.* 304:1 (1986)
108. Alcock C, et al. *Astrophys. J.* 542:281 (2000)
109. Hamadache C, et al. *Astron. Astrophys.* 454:185 (2006)
110. Wyrzykowski L, et al. *Mon. Not. R. Astron. Soc.* 397:1228 (2009); Calchi Novati S, Mancini L, Scarpetta G, Wyrzykowski L. *Mon. Not. R. Astron. Soc.* 400:1625 (2009); Wyrzykowski L, et al. *Mon. Not. R. Astron. Soc.* 407:189 (2010); Wyrzykowski L, et al. *Mon. Not. R. Astron. Soc.* 413:493 (2011); Wyrzykowski L, et al. *Mon. Not. R. Astron. Soc.* 416:2949 (2011)
111. Niikura H, et al. *Phys. Rev. D* 99:083503 (2019)
112. Zumalacárregui M, Seljak U. *Phys. Rev. Lett.* 121:141101 (2018)
113. García-Bellido J, Clesse S, Fleury P. *Phys. Dark Univ.* 20:95 (2018)
114. Oguri M, et al. *Phys. Rev. D* 97:023518 (2018)
115. Dalcanton JJ, et al. *Astrophys. J.* 424:550 (1994)
116. Mediavilla E, et al. *Astrophys. J.* 706:1451 (2009)
117. Wilkinson PN, et al. *Phys. Rev. Lett.* 86:584 (2001)
118. Roncadelli M, Treves A, Turolla R. arXiv:0901.1093 [astro-ph.CO] (2009)
119. Capela F, Pshirkov M, Tinyakov P. *Phys. Rev. D* 87:023507 (2013)
120. Capela F, Pshirkov M, Tinyakov P. *Phys. Rev. D* 87:123524 (2013)
121. Pani P, Loeb A. *J. Cosmol. Astropart. Phys.* 1406:026 (2014)
122. Defillon G, Granet E, Tinyakov P, Tytgat MHG. *Phys. Rev. D* 90:103522 (2014)
123. Ibata R, et al. *Mon. Not. R. Astron. Soc.* 428:3648 (2013)
124. Graham PW, Rajendran S, Varela J. *Phys. Rev. D* 92:063007 (2015)
125. Montero-Camacho P, et al. *J. Cosmol. Astropart. Phys.* 1908:031 (2019)
126. Carr BJ, Sakellariadou M. *Astrophys. J.* 516:195 (1999)
127. Bahcall JN, Hut P, Tremaine S. *Astrophys. J.* 290:15 (1985)
128. Weinberg MD, Shapiro SL, Wasserman I. *Astrophys. J.* 312:367 (1987)
129. Quinn DP, et al. *Mon. Not. R. Astron. Soc.* 396:11 (2009)
130. Monroy-Rodríguez MA, Allen C. *Astrophys. J.* 790:159 (2014)
131. Tian HJ, El-Badry K, Rix HW, Gould A. *Astrophys. J.* 246:4 (2020)
132. Moore B. *Astrophys. J. Lett.* 413:L93 (1993)
133. Brandt TD. *Astrophys. J.* 824:L31 (2016)
134. Koushiappas SM, Loeb A. *Phys. Rev. Lett.* 119:041102 (2017)
135. Stegmann J, Capelo PR, Bortolas E, Mayer L. *Mon. Not. R. Astron. Soc.* 492:5247 (2020)
136. Lacey CG, Ostriker JP. *Astrophys. J.* 299:633 (1985)
137. Carr BJ. *Comments Astrophys. Space Phys.* 7:161 (1978)
138. Afshordi N, McDonald P, Spergel DN. *Astrophys. J. Lett.* 594:L71 (2003); Murgia R, Scelfo G, Viel M, Raccanelli A. *Phys. Rev. Lett.* 123:071102 (2019)
139. Bondi H. *Mon. Not. R. Astron. Soc.* 112:195 (1952)
140. Carr BJ. *Mon. Not. R. Astron. Soc.* 189:123 (1979)
141. Salpeter E. *Astrophys. J.* 140:796 (1964)
142. Sołtan A. *Mon. Not. R. Astron. Soc.* 200:115 (1982)
143. Ricotti M, Ostriker JP, Mack KJ. *Astrophys. J.* 680:829 (2008); Ricotti M. *Astrophys. J.* 662:53 (2007); Mack KJ, Ostriker JP, Ricotti M. *Astrophys. J.* 665:1277 (2007)
144. Ali-Haïmoud Y, Kamionkowski M. *Phys. Rev. D* 95:043534 (2017)
145. Horowitz B. arXiv:1612.07264 [astro-ph.CO] (2016)
146. Poulin V, et al. *Phys. Rev. D* 96:083524 (2017); Serpico PD, Poulin V, Inman D, Kohri K. *Phys. Rev. Res.* 2:023204 (2020)
147. Gaggero D, et al. *Phys. Rev. Lett.* 118:241101 (2017)
148. Manshanden J, et al. *J. Cosmol. Astropart. Phys.* 1906:026 (2019)
149. Inoue Y, Kusenko A. *J. Cosmol. Astropart. Phys.* 1710:034 (2017); Lu P, et al. arXiv:2007.02213 [astro-ph.CO] (2020)

Annu. Rev. Nucl. Part. Sci. 2020.70:355-394. Downloaded from www.annualreviews.org
Access provided by WIB6263 - Deutsches Elektronen Synchroton (DESY) on 04/08/21. See copyright for approved use.

150. De Luca V, Franciolini G, Pani P, Riotto A. arXiv:2003.12589 [astro-ph.CO] (2020)
151. Chluba J, Erickcek AL, Ben-Dayan I. *Astrophys. J.* 758:76 (2012)
152. Barrow JD, Coles P. *Mon. Not. R. Astron. Soc.* 248:52 (1991)
153. Kohri K, Nakama T, Suyama T. *Phys. Rev. D* 90:083514 (2014)
154. Nakama T, Suyama T, Yokoyama J. *Phys. Rev. D* 94:103522 (2016)
155. Nakama T, Carr B, Silk J. *Phys. Rev. D* 97:043525 (2018)
156. Abitbol MH, Chluba J, Hill JC, Johnson BR. *Mon. Not. R. Astron. Soc.* 471:1126 (2017)
157. Abbott BP, et al. *Phys. Rev. Lett.* 116:061102 (2016); Abbott BP, et al. *Phys. Rev. Lett.* 116:241103 (2016); Abbott BP, et al. *Astrophys. J. Lett.* 833:L1 (2016); Abbott B, et al. *Phys. Rev. X* 9:031040 (2019)
158. Abbott BP, et al. *Astrophys. J.* 659:918 (2007)
159. Abbott BP, et al. *Phys. Rev. Lett.* 121:231103 (2018)
160. Abbott BP, et al. *Phys. Rev. Lett.* 123:161102 (2019)
161. Carr BJ. *Astron. Astrophys.* 89:6 (1980)
162. Wang S, Wang YF, Huang QG, Li TGF. *Phys. Rev. Lett.* 120:191102 (2018)
163. Raidal M, Spethmann C, Vaskonen V, Veerme H. *J. Cosmol. Astropart. Phys.* 1902:018 (2019)
164. Vaskonen V, Veerme H. *Phys. Rev. D* 101:043015 (2020)
165. Chen ZC, Yuan C, Huang QG. arXiv:1910.12239 [astro-ph.CO] (2019)
166. Bartolo N, et al. *J. Cosmol. Astropart. Phys.* 2002:028 (2020)
167. Saito R, Yokoyama J. *Phys. Rev. Lett.* 102:161101 (2009)
168. Saito R, Yokoyama J. *Prog. Theor. Phys.* 123:867 (2009)
169. Bugaev E, Klimai P. *Phys. Rev. D* 81:023517 (2010)
170. Assadullahi H, Wands D. *Phys. Rev. D* 81:023527 (2010); Bugaev E, Klimai P. *Phys. Rev. D* 83:083521 (2011)
171. Nakama T, Suyama T. *Phys. Rev. D* 92:121304 (2015); Nakama T, Suyama T. *Phys. Rev. D* 94:043507 (2016)
172. Ballesteros G, Serpico PD, Taoso M. *J. Cosmol. Astropart. Phys.* 1810:043 (2018)
173. Kühnel F, Matas A, Starkman GD, Freese K. arXiv:1811.06387 [gr-qc] (2018)
174. Gondolo P, Silk J. *Phys. Rev. Lett.* 83:1719 (1999)
175. Shemmer O, et al. *Astrophys. J.* 614:547 (2004)
176. Carr B, Kühnel F, Visinelli L. arXiv:2008.08077 [astro-ph.CO] (2020)
177. Hasegawa F, Kawasaki M. *Phys. Rev. D* 98:043514 (2018)
178. Mediavilla E, et al. *Astrophys. J.* 836:L18 (2017)
179. Wyrzykowski L, Mandel I. *Astron. Astrophys.* 636:A20 (2020)
180. Brown G, Lee C, Bethe H. arXiv:astro-ph/9909270 (1999)
181. Cappelluti N, et al. *Astrophys. J.* 769:68 (2013)
182. Clesse S, García-Bellido J. *Phys. Dark Univ.* 22:137 (2018)
183. Silk J. *Astrophys. J.* 839:L13 (2017)
184. Kusenko A, et al. arXiv:2001.09160 [astro-ph.CO] (2020)
185. van Elteren A, et al. *Astron. Astrophys.* 624:A120 (2019)
186. Calcino J, García-Bellido J, Davis TM. *Mon. Not. R. Astron. Soc.* 479:2889 (2018)
187. Hawkins MRS. *Astron. Astrophys.* 575:A107 (2015)
188. Chisholm JR. *Phys. Rev. D* 73:083504 (2006)
189. Hawkins MRS. *Nature* 366:242 (1993)
190. Hawkins M. *Astron. Astrophys.* 462:581 (2007)
191. Hawkins MRS. *Astron. Astrophys.* 633:A107 (2020)
192. Vedantham HK, et al. *Astrophys. J.* 845:89 (2017)
193. Ipser JR, Semenzato R. *Astron. Astrophys.* 149:408 (1985)
194. Carlberg RG, Dawson PC, Hsu T, Vandenberg DA. *Astrophys. J.* 294:674 (1985); Strömgren B. An investigation of the relations between age, chemical composition and parameters of velocity distribution based on *uvbyβ* photometry of F stars within 100 parsec. In *The Galaxy*, ed. G Gilmore, B Carswell, pp. 229–46. Dordrecht, Neth.: D. Reidel Publ. Co. (1987); Gomez AE, et al. *Astron. Astrophys.* 236:95 (1990)

Annu. Rev. Nucl. Part. Sci. 2020.70:355-394. Downloaded from www.annualreviews.org
Access provided by WIB6263 - Deutsches Elektronen Synchroton (DESY) on 04/08/21. See copyright for approved use.

195. Lacey CG. The disc heating problem. In *Dynamics of Disc Galaxies*, ed. B Sundelius, pp. 257–78. Gothenburg, Swed.: Univ. Gothenburg (1991)
196. Fuller GM, Kusenko A, Takhistov V. *Phys. Rev. Lett.* 119:061101 (2017)
197. Abramowicz MA, Bejger M, Wielgus M. *Astrophys. J.* 868:17 (2018)
198. Kashlinsky A, Arendt RG, Mather J, Moseley SH. *Nature* 438:45 (2005); Kashlinsky A, et al. *Rev. Mod. Phys.* 90:025006 (2018); Kashlinsky A. *Astrophys. J.* 823:L25 (2016)
199. Ioka K, Tanaka T, Nakamura T. *Phys. Rev. D* 60:083512 (1999)
200. Inoue KT, Tanaka T. *Phys. Rev. Lett.* 91:021101 (2003)
201. Clesse S, García-Bellido J. *Phys. Dark Univ.* 15:142 (2017)
202. Blinnikov S, Dolgov A, Porayko N, Postnov K. *J. Cosmol. Astropart. Phys.* 1611:036 (2016)
203. Fernandez N, Profumo S. *J. Cosmol. Astropart. Phys.* 1908:022 (2019)
204. Gerosa D, et al. *Phys. Rev. D* 98:084036 (2018)
205. García-Bellido J. *J. Phys. Conf. Ser.* 840:012032 (2017)
206. Dolgov A, et al. arXiv:2005.00892 [astro-ph.CO] (2020)
207. Bartolo N, et al. *Phys. Rev. D* 99:103521 (2019); Bartolo N, et al. *Phys. Rev. Lett.* 122:211301 (2019)
208. Cai RG, Pi S, Sasaki M. *Phys. Rev. Lett.* 122:201101 (2019)
209. Kormendy J, Ho LC. *Annu. Rev. Astron. Astrophys.* 51:511 (2013); Pardo K, et al. *Astrophys. J.* 831:203 (2016); Baldassare VF, Reines AE, Gallo E, Greene JE. *Astrophys. J.* 836:20 (2017)
210. Law-Smith J, et al. *Astrophys. J.* 841:132 (2017)
211. Inoue KT, Chiba M. *Astrophys. J.* 591:L83 (2003); Inoue KT, Rashkov V, Silk J, Madau P. *Mon. Not. R. Astron. Soc.* 435:2092 (2013)
212. Ezquiaga JM, García-Bellido J, Ruiz Morales E. *Phys. Lett. B* 776:345 (2018); García-Bellido J, Ruiz Morales E. *Phys. Dark Univ.* 18:47 (2017)
213. Bezrukov F, Pauly M, Rubio J. *J. Cosmol. Astropart. Phys.* 1802:040 (2018)
214. García-Bellido J, Carr B, Clesse S. arXiv:1904.11482 [astro-ph.CO] (2019)
215. Kruijssen JMD, Lutzgendorf N. *Mon. Not. R. Astron. Soc.* 434:41 (2013)
216. Sakharov AD. *Pisma Zh. Eksp. Teor. Fiz.* 5:32 (1967) [*Usp. Fiz. Nauk.* 161:61 (1991)]
217. Asaka T, Grigoriev D, Kuzmin V, Shaposhnikov M. *Phys. Rev. Lett.* 92:101303 (2004)
218. Shaposhnikov M. Baryogenesis. In *Particle Physics: Ideas and Recent Developments*, ed. JJ Aubert, R Gastmans, JM Gérard, pp. 397–416. Dordrecht, Neth.: Springer (2000)
219. Eroshenko YN. *Astron. Lett.* 42:347 (2016) [*Pisma Astron. Zh.* 42:359 (2016)]
220. Boucenna SM, Kühnel F, Ohlsson T, Visinelli L. *J. Cosmol. Astropart. Phys.* 1807:003 (2018)
221. Bertschinger E. *Astrophys. J. Suppl.* 58:39 (1985)
222. Adamek J, Byrnes CT, Gosenca M, Hotchkiss S. *Phys. Rev. D* 100:023506 (2019)
223. Cirelli M, Panci P, Serpico PD. *Nucl. Phys. B* 840:284 (2010)
224. Cirelli M, et al. *J. Cosmol. Astropart. Phys.* 1103:051 (2011). Erratum. *J. Cosmol. Astropart. Phys.* 1210:E01 (2012)
225. Kühnel F, Ohlsson T. *Eur. Phys. J. C* 79:687 (2019)
226. Kühnel F, Ohlsson T. *Phys. Rev. D* 96:103020 (2017)
227. Kühnel F, Ohlsson T. Primordial black-hole signatures in neutrino telescopes. In *Probing Particle Physics with Neutrino Telescopes*, ed. C Pérez de los Heros, pp. 401–18. Singapore: World Sci. (2020)
228. MacGibbon JH. *Nature* 329:308 (1987)
229. Barrow JD, Copeland EJ, Liddle AR. *Phys. Rev. D* 46:645 (1992); Alexander S, Mészáros P. arXiv:hep-th/0703070 (2007); Fujita T, Kawasaki M, Harigaya K, Matsuda R. *Phys. Rev. D* 89:103501 (2014)
230. Lehmann BV, Johnson C, Profumo S, Schwemberger T. *J. Cosmol. Astropart. Phys.* 1910:046 (2019)
231. Chen P, Adler RJ. *Nucl. Phys. Proc. Suppl.* 124:103 (2003)
232. Carr B. *Mod. Phys. Lett. A* 28:1340011 (2013)
233. Carr BJ, Mureika J, Nicolini P. *J. High Energy Phys.* 1507:52 (2015)
234. Dvali G, Gomez C. *Fortsch. Phys.* 61:742 (2013)
235. Kühnel F, Sandstad M. *Phys. Rev. D* 92:124028 (2015)
236. Dvali G, Eisemann L, Michel M, Zell S. arXiv:2006.00011 [hep-th] (2020)
237. Abbott BP, et al. *Astrophys. J. Lett.* 892:L3 (2020); Abbott R, et al. *Astrophys. J. Lett.* 896:L44 (2020)
238. Abbott R, et al. *Phys. Rev. Lett.* 125:101102 (2020); Abbott R, et al. *Astrophys. J. Lett.* 900:L13 (2020)

Annu. Rev. Nucl. Part. Sci. 2020.70:355-394. Downloaded from www.annualreviews.org
Access provided by WIB6263 - Deutsches Elektronen Synchroton (DESY) on 04/08/21. See copyright for approved use.

Annual Review of Nuclear and Particle Science

Volume 70, 2020

Contents

Annu. Rev. Nucl. Part. Sci. 2020.70:355-394. Downloaded from www.annualreviews.org
Access provided by WIB6263 - Deutsches Elektronen Synchroton (DESY) on 04/08/21. See copyright for approved use.

Errata

An online log of corrections to *Annual Review of Nuclear and Particle Science* articles may be found at http://www.annualreviews.org/errata/nucl

Annu. Rev. Nucl. Part. Sci. 2020.70:355-394. Downloaded from www.annualreviews.org
Access provided by WIB6263 - Deutsches Elektronen Synchroton (DESY) on 04/08/21. See copyright for approved use.